

Sound Field Synthesis With Higher-Order Ambisonics

**Internship of second year Master IMDEA:
International Master's Degree in Electro Acoustics
written by:**

Samuel Dupont

Master student

February 8th to June 10th 2016 under the guidance of:

Alain Berry
Manuel Melon
Philippe-Aubert Gauthier
Pierre Lecomte

Company referee, professor
Academic referee, professor
Research Associate
PhD student

Internship performed at:

GROUPE D'ACOUSTIQUE DE L'UNIVERSITÉ DE SHERBROOKE (GAUS),
UNIVERSITÉ DE SHERBROOKE, QUÉBEC, CANADA

Home institution:

FACULTY OF SCIENCE
UNIVERSITÉ DU MAINE, LE MANS, FRANCE

Contents

1	Introduction	2
1.1	Company presentation	2
1.2	Context and aim of the work	2
1.3	Literature review	3
2	Mathematical and acoustic background	5
2.1	System of coordinates	5
2.2	Fundamental equation for Higher Order Ambisonics	5
2.3	Spherical harmonics	6
3	On the use of Higher Order Ambisonics	8
3.1	A continuous recording approach of the sound field encoding	9
3.1.1	Integration over a rigid sphere	9
3.2	A continuous reproduction approach for the sound field reconstruction	11
3.3	Spatial sampling of the sphere	12
3.3.1	Encoding	12
3.3.2	Signals decoding: Basic decoding methods	14
3.4	Ambisonics reconstruction of a spherical source	14
4	Experiments: Materials and methods	17
4.1	Uniform rectangular microphone array	17
4.2	Spherical microphone array	17
4.3	Microphone calibration	18
4.4	Post-processing of recorded signals	19
4.5	Results for the spherical microphone array measurements	19
5	Experiments in an anechoic environment	22
5.1	Uniform rectangular array measurements: Time-domain approach . .	22
5.2	Uniform rectangular array: Frequency-domain approach	23
5.3	Spherical microphone array	27
5.3.1	Discussion of Memsbedev and plane antenna results	30
6	Conclusion	31
7	Acknowledgement	32
A	Appendix	34
A.1	Demonstration of the integration on a rigid sphere	34
A.2	Demonstration of monopole encoding	35
A.3	Matlab program	35
B	Appendix Constructions	36
B.1	Spherical array of loudspeakers	36
B.2	Uniform rectangular array	37

Chapter 1

Introduction

1.1 Company presentation

Founded in 1984 and directed for 12 years by Prof. Jean Nicolas, the GAUS is the 1st academic acoustics and vibration research laboratory in Canada, and one of the most important academic research centers in the world for noise and vibration control. In 2009, the GAUS celebrated 25 years of successful acoustic research and development.

The current director is Alain Berry. In 2012, the GAUS inaugurates its new laboratory and acquires many new equipments to study larger structures.



1.2 Context and aim of the work

This report accounts for a master internship of five months on Sound field synthesis. It is actually focused on higher order Ambisonics. The aim is to assess the good physical performance of an Ambisonics system through theoretical simulations and measurements.

The set-up is an Ambisonic sphere based on Lebedev sphere discretisation shown on Fig 1.1.

This work was done in collaboration with Pierre Lecomte, a PhD student working on Ambisonics and active room compensation.

The chapter 2 of the report gives the mathematical and acoustic background used as basis in this report. Next, theory of Higher-Order Ambisonics (HOA) will be seen in chapter 3, through formulas and simulations. This part follows a linear development from a purely theoretical approach of the problem toward a physical implementation. It also presents the general behaviour of the HOA, as well as the different limitations.

Then toward a real implementation, the equipments and the method used to measure the reproduced sound fields will be presented in chapter 4.

Finally, the measurement with the system will be presented in chapter 5 presenting the assessment of the Ambisonics sphere in an anechoic space. The acoustical measurements have been done with a spherical microphone and a planar microphone antenna, both ways will be compared and discussed.

Both types of measurements are compared and discussed.

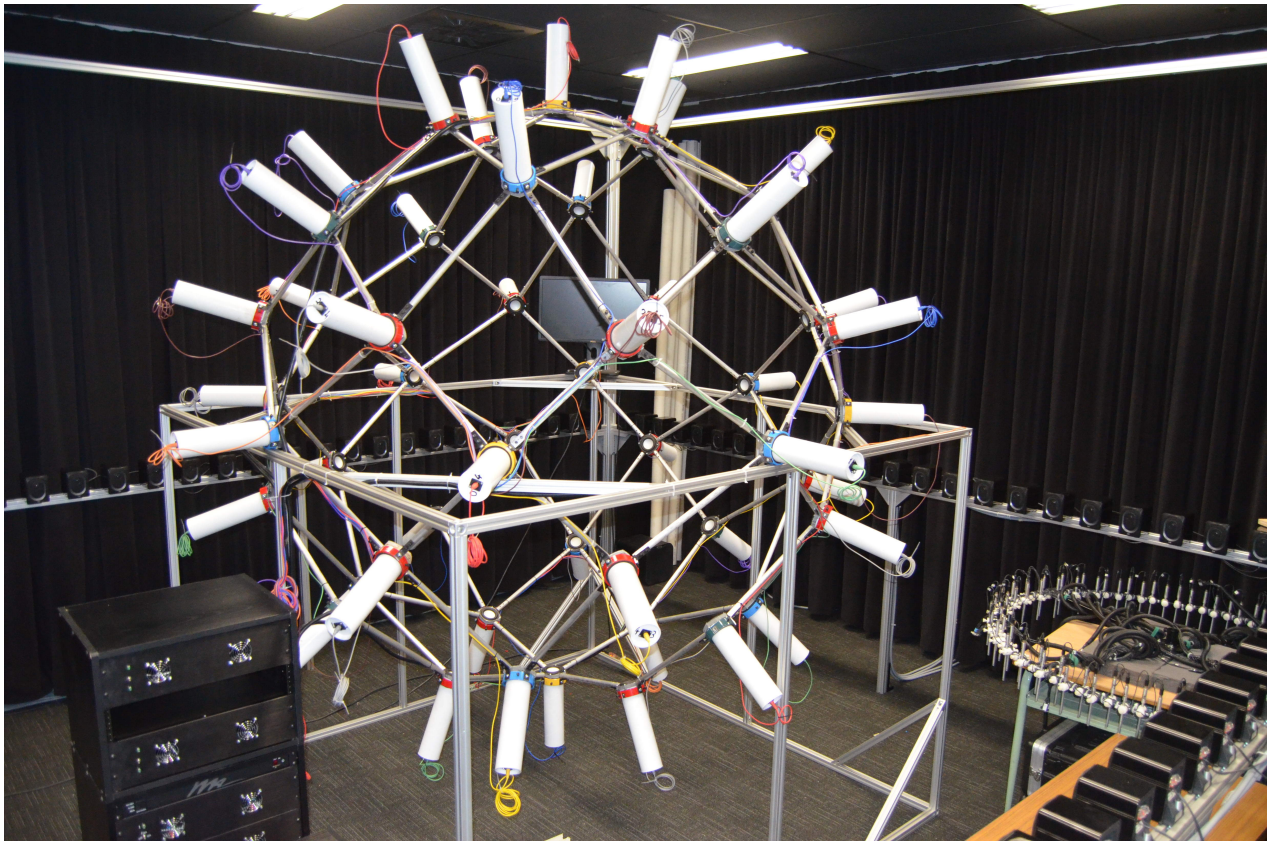


Figure 1.1: Spherical arrangement of 50 loudspeakers according to a Lebedev grid.

1.3 Literature review

The Ambisonics approach is based on decomposition of the acoustic field on the different orders of spherical harmonics centered at the listener position.

One of the main interests of sound field reproduction using Ambisonics is to be able through a low order encoding, to reproduce spatial information which can be decoded simply and quickly. Furthermore, the encoding is completely independent of the decoding, which makes Ambisonics a very flexible approach.

The first works on Ambisonics were developed by Michael Gerzon in 1973 [1]. However, this was limited to the first order of spherical harmonics expansion. Next Bamford in 1995 [2] and Jérôme Daniel in 2000 [3], developed the idea of HOA. The sound field synthesis was in that time motivated by the constraints of reproducing a real acoustic field with a minimal set-up, dealing with the data flow (CPU power, transmission).

In the following years several researches were conducted on HOA. Among these the works of Sébastien Moreau [4], Franz Zotter, Noisterning, Paoletti, Filippo Maria Fazi [5] where trying to overcome the limitation induced by encoding and decoding of Ambisonics signal and set-up.

These researches aimed at the improvement of the quality of spatial restitution over a larger area and span of frequency. Also, the aim was to allow modifications of the signal in between recording and decoding, directly in the ambisonics domain.

In the internship, the set-up and the work performed is directly related to Pierre Lecomte works on Lebedev spherical mesh [6].

Chapter 2

Mathematical and acoustic background

The aim of this chapter is to provide a short introduction on the mathematical and acoustical tools used in this internship. These tools are the basis of the theoretical and experimental works presented in this report.

2.1 System of coordinates

Coordinates are shown in Fig.2.1. The azimuth angle θ is measured from the x-axis towards the y-axis, while the elevation angle σ is measured upwards from the x-y plane.

A position (r, θ, σ) represented in spherical coordinates can be related to the same position represented in Cartesian coordinates (x, y, z) using:

$$\begin{aligned} x &= r \cos \theta \cos \sigma \\ y &= r \sin \theta \cos \sigma \\ z &= r \sin \theta. \end{aligned} \tag{2.1}$$

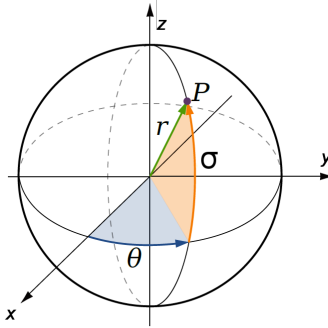


Figure 2.1: Spherical coordinate system defined relative to the Cartesian coordinate system.

2.2 Fundamental equation for Higher Order Ambisonics

Ambisonics are based on the solution of the wave equation written in spherical coordinates:

$$\left[\frac{1}{r^2} \frac{\partial}{\partial r} \left(r^2 \frac{\partial}{\partial r} \right) + \frac{1}{r^2 \sin \theta} \frac{\partial}{\partial \theta} \left(\sin \theta \frac{\partial}{\partial \theta} \right) + \frac{1}{r^2 \sin^2 \theta} \frac{\partial^2}{\partial \sigma^2} - \frac{1}{c^2} \frac{\partial^2}{\partial t^2} \right] p(r, \theta, \sigma, t) = 0. \tag{2.2}$$

Since the differential wave equation admits a variable separation, the solution is obtained as described below [7].

Considering the interior problem [8], all the sources are outside a spherical volume of radius a . Thus, for $r < a$ the sound field can be written as a Fourier-Bessel series, at all point (r, θ, σ) , for a centered region where the pressure p is not infinite (see [4]):

$$p(r, \theta, \sigma, t) = \sum_{m=0}^{\infty} (2m+1)i^m J_m(kr) \sum_{n=-m}^m B_{mn} Y_{mn}(\theta, \sigma) e^{j\omega t}, \quad (2.3)$$

where k is the wave number defined by ω/c , $\omega = 2\pi f$, c the celerity of sound in air medium.

Functions $Y_{mn}(\theta, \sigma)$ are spherical harmonics and represent the angular dependency of the sound field. J_m and B_{mn} represent the spherical Bessel functions and the Ambisonics coefficient, respectively.

2.3 Spherical harmonics

In this section, the spherical harmonics are represented as a set of orthonormal basis functions defined as:

$$Y_{mn}(\theta, \sigma) = \tilde{P}_{mn}(\sin(\sigma)) \times \begin{cases} \cos(n\theta) & \text{if } n \geq 0 \\ \sin(n\theta) & \text{if } n < 0 \end{cases}, \quad (2.4)$$

where \tilde{P}_{mn} represents the associated Legendre functions defined as:

$$P_{mn}(\eta) = (-1)^n (1 - \eta^2)^{\frac{n}{2}} \frac{\partial^n}{\partial \eta^n} P_m(\eta), \quad 0 < n < m \quad (2.5)$$

with

$$P_m(\eta) = \frac{1}{2^m m!} \frac{\partial^m}{\partial \eta^m} (\eta^2 - 1)^m, \quad (2.6)$$

where $\epsilon_0 = 1$, $\epsilon_n = 2$ $n > 0$.

In the following, normalised spherical harmonics N3D [4] will be used:

$$\tilde{Y}_{mn}(\theta, \sigma) = \sqrt{\epsilon_n (2m+1) \frac{(m-n)!}{(m+n)!}} P_{mn}(\sin \sigma) \times \begin{cases} \cos(n\theta) & \text{if } n \geq 0 \\ \sin(n\theta) & \text{if } n < 0 \end{cases}. \quad (2.7)$$

Spherical harmonics form an orthonormal basis, thus using the spherical scalar product $\langle f, g \rangle$ we have:

$$\langle \tilde{Y}_{mn}(\theta, \sigma), \tilde{Y}_{m'n'}(\theta', \sigma') \rangle = \frac{1}{4\pi} \int_{\theta=0}^{2\pi} \int_{\sigma=\frac{-pi}{2}}^{\frac{pi}{2}} \tilde{Y}_{mn}(\theta, \sigma) \tilde{Y}_{m'n'}(\theta, \sigma) d\theta d\sigma = \delta_{mm'} \delta_{nn'}. \quad (2.8)$$

In the sequel, the spherical normalised integration in Eq. 2.8 will be discretised using a weighted Lebedev quadrature rule.

The following Fig 2.2 shows a representation of the spherical harmonics of order 0 to 3. It can be seen on them the angular dependency of the function traduced later in the B_{mn} coefficient.

Note that the spherical harmonics have a complex exponential dependence on σ , so that the absolute value, $|\tilde{Y}_{mn}(\theta, \sigma)|$, will be constant along σ . Therefore, plots of the real and imaginary parts of the spherical harmonics are typically presented, rather than plots of the magnitude and phase.

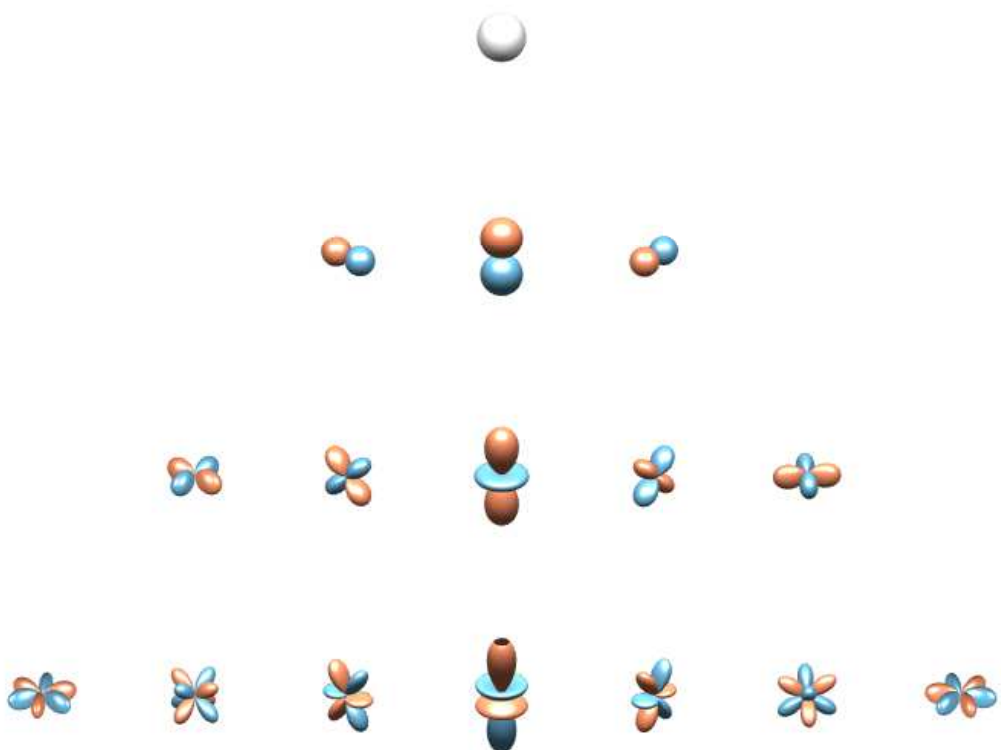


Figure 2.2: Balloon plots of the spherical harmonics for $M = 0$ (top row) to $M = 3$ (bottom row), $\Im\{\tilde{Y}_{mn}(\theta, \sigma)\}$ for $-n \leq m \leq -1$ are presented in the left-hand side columns, and $\Re\{\tilde{Y}_{mn}(\theta, \sigma)\}$ for $0 \leq m \leq n$ are presented in the right-hand side columns. Colors indicate the sign of the spherical harmonic functions, with red shades representing positive values, and blue shades representing negative values, program link.

Chapter 3

On the use of Higher Order Ambisonics

This chapter presents the recording, Ambisonics encoding, and Ambisonics decoding of a pressure field using Near-Field Compensated Higher-Order Ambisonics (NFC-HOA).

These topics are covered by a step-by-step presentation. Starting from a continuous formulation, including the ideal case of an infinite number of reproduction sources on a sphere (recording and reproduction), to the physical discrete domain which corresponds to the actual implementation.

The main point of Ambisonics is to obtain the HOA coefficients B_{mn} . They are spherical harmonics signals that represent the incoming spatial distribution of the sound. Once they are obtained, the final aim is to decode them using the reproduction system.

Fig. 3.1 shows a schematical representation of the different steps of the processing chain. Each of these steps are presented in the forthcoming sections.

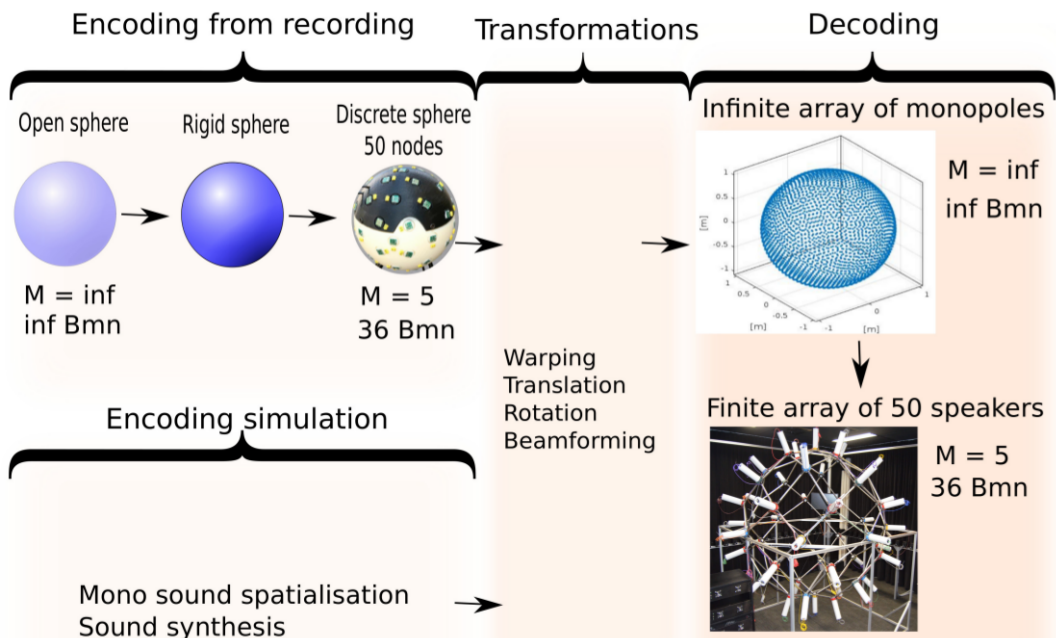


Figure 3.1: Typical HOA signal processing chain.

3.1 A continuous recording approach of the sound field encoding

The Ambisonics method is characterised by its ability to record a sound field in three dimensions using spherical sampling of sound fields at a given radius. Considering an open sphere of radius r in any given sound pressure field, described by Eq. 2.3, one notes that the sound field can be described by the B_{mn} coefficients only.

In order to evaluate these coefficients, the projection of the pressure $p(kr, \theta, \sigma)$ over the spherical harmonics is considered:

$$\langle p(kr, \theta, \sigma), Y_{mn}(\theta, \sigma) \rangle = \frac{1}{4\pi} \int_{\theta=0}^{2\pi} \int_{\sigma=-\frac{\pi}{2}}^{\frac{\pi}{2}} p(kr, \theta, \sigma) \tilde{Y}_{mn}(\theta, \sigma) \cos(\sigma) d\theta d\sigma, \quad (3.1)$$

replacing $p(kr, \theta, \sigma)$ by its expression Eq. 2.3, in Eq. 3.1, one obtains:

$$\langle p(kr, \theta, \sigma), Y_{mn}(\theta, \sigma) \rangle = \frac{1}{4\pi} \sum_{m'=0}^{\infty} i^{m'} J_{m'}(kr) \sum_{n'=0}^{m'} B_{m'n'} \int_{\theta=0}^{2\pi} \int_{\sigma=-\frac{\pi}{2}}^{\frac{\pi}{2}} \tilde{Y}_{m'n'}(\theta, \sigma) \tilde{Y}_{mn}(\theta, \sigma) \cos(\sigma) d\theta d\sigma. \quad (3.2)$$

One simplifies the previous equation using the orthonormality of spherical harmonics to find the Ambisonics coefficients B_{mn} :

$$B_{mn} = (i^m J_m(kr))^{-1} \langle p(kr, \theta, \sigma), Y_{mn}(\theta, \sigma) \rangle. \quad (3.3)$$

Thus, if the sound pressure field over an open spherical surface of radius r is known, it is possible to calculate the Ambisonics coefficients. In order to do so, one first projects the acoustical pressure on the spherical harmonics. Second, the multiplication of the results by $(i^m J_m(kr))^{-1}$ gives the Ambisonics coefficients.

As the B_{mn} are derived from a Fourier-Bessel series, one needs an infinite number of coefficients to obtain a complete representation of the sound field. As shown above, these coefficients are related to the spherical harmonics, there are $(2m + 1)$ coefficients for each order m . The letter M will refer to the maximum order set used in the Fourier-Bessel series.

Although the infinite set of coefficients B_{mn} can provide a complete description of $p(r, \theta, \sigma)$, it is reminded that J_m are oscillating functions. Therefore they cross zero at some frequencies for some radius. This is exemplified in Fig. 3.2.

In order to overcome this issue, different solutions have been proposed. They are summarized by Rafaely in [9]. However, in this work, the integration over a rigid sphere will be the sole investigated solution. Note that this solution corresponds to the spherical microphone array that was available for the experiments.

3.1.1 Integration over a rigid sphere

An approach to improve the continuous spherical microphone singularities is to introduce a rigid sphere at the microphone radius and take into account the diffracted sound pressure field. Thankfully, the analytical solution of the sound diffraction by a rigid sphere is readily available.

Assuming a rigid sphere radius a in an acoustic pressure field, the resulting acoustic pressure field p_{tot} is given by the sum of the direct pressure p_{dir} (without the

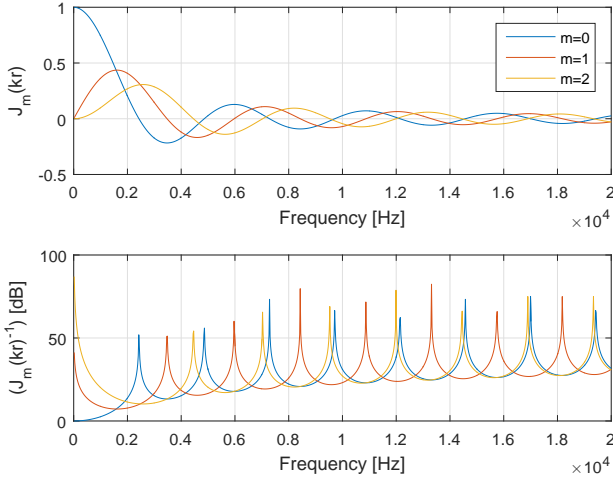


Figure 3.2: Spherical Bessel functions (top) and their reciprocal values (bottom) for an audio bandwidth with sphere radius set to 7 cm, program link.

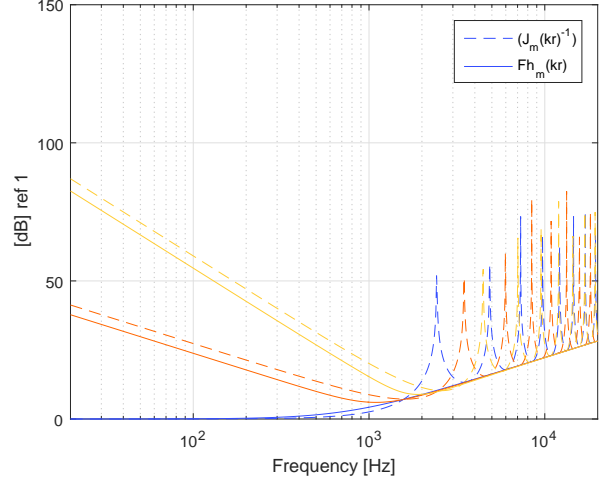


Figure 3.3: Comparison of equalisation filters for different orders ($m=0$ blue, $m=1$ red, $m=2$ yellow), r fixed to 7 cm, program link.

diffracting sphere) and the diffracted sound pressure field p_{dif} :

$$p_{tot}(kr, \theta, \sigma) = p_{dir}(kr, \theta, \sigma) + p_{dif}(kr, \theta, \sigma) \quad (3.4)$$

The resulting pressure can be written using Fourier-Bessel series as:

$$p_{tot}(r, \theta, \sigma) = \sum_{m,n,\sigma} i^m \tilde{Y}_{mn}(\theta, \sigma) (B_{mn} J_m(kr) + D_{mn} H_m^{(2)}(kr)), \quad (3.5)$$

where B_{mn} and D_{mn} are the spherical coefficients of the direct field and the diffracted field respectively and $H_m^{(2)}$ the spherical Hankel functions of the second kind. Using Eq. (3.5) with some adjustments (complete demonstration is provided in Appendix A.1), the B_{mn} coefficients can be determined on the sphere surface by:

$$B_{mn} = Fh_m \langle p(ka, \theta, \sigma), \tilde{Y}_{mn}(\theta, \sigma) \rangle, \quad (3.6)$$

with

$$Fh_m = i^{-(m-1)} (ka)^2 H_m'^{(2)}(ka). \quad (3.7)$$

Figure 3.3 shows a comparison between the rigid-sphere (Eq.(3.7)) and open-sphere (Eq. (3.3)) equalisation filters. It is clear that the equalization filter for the rigid sphere does not suffer from singularities. However, except for zeroth order, the large gain for the low frequency remains for the rigid sphere.

On practical ground, this might turn out to be a problem for sound field reproduction. For example at the second order at 100 Hz, for the rigid sphere, the signal gain goes up to 55 dB. For the open sphere 59 dB. A solution is to limit the gain up to a given level. This is discussed in Sec. 4.5.

3.2 A continuous reproduction approach for the sound field reconstruction

In this section, an infinite number of point sources distributed along a sphere of radius r_{hp} is considered. The B_{mn} coefficients are derived from the precedent continuous encoding approach.

The aim is to use the constructive and destructive interferences of all the point sources in order to reconstruct the sound pressure field encoded by B_{mn} coefficients. Thus it is mandatory to take into account the near-field effect of these point sources. Therefore, the first step is the consideration for an encoding of a spherical source located in $(r_{hp}, \theta_{hp}, \sigma_{hp})$ (details are provided in Appendix A.2):

$$B_{mn} = SF_m(kr_{hp})\tilde{Y}_{mn}(\theta_{hp}, \sigma_{hp}), \quad (3.8)$$

where S is the amplitude of the point source and $F_m(kr_{hp})$ are the near-field filters that characterize the acoustic propagation from the reproduction source, including near-field effects. Also, a new set of equalization filters are provided:

$$F_m(kr_{hp}) = -i^{(-m+1)} \frac{k}{4\pi} H_m^{(2)}(kr_{hp}). \quad (3.9)$$

The near-field effect of the reproduction points sources will thus, be compensated by the inverse filters:

$$F_m^{-1}(kr_{hp}) = \frac{1}{F_m(kr_{hp})}. \quad (3.10)$$

The Figure 3.4 shows the filters for r_{hp} fixed at 1.07 m, this corresponds to the radius of the sphere used for the experiments later described in this report. In comparison with the encoding equalization filters, one notes that they have a positive effect in terms of gain limitation in the low frequency range.

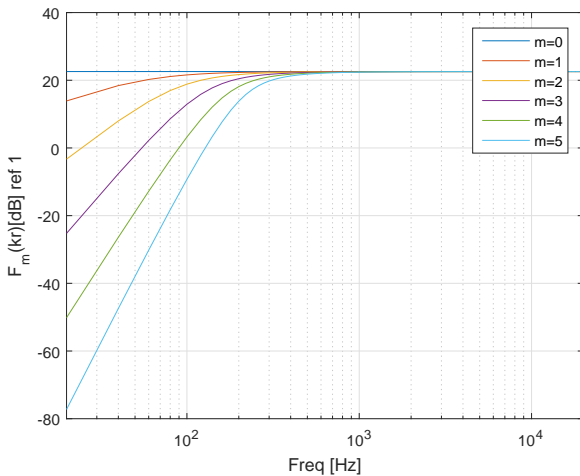


Figure 3.4: Near field compensation filter, $F_m(kr_{hp})$, program link.

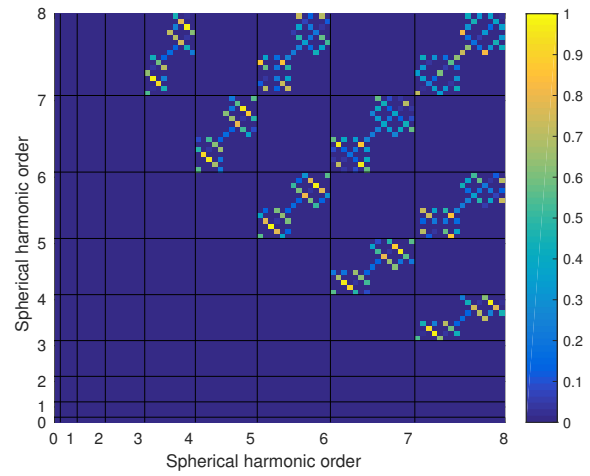


Figure 3.5: Orthogonality error of Lebedev 50 nodes program link.

3.3 Spatial sampling of the sphere

In actual application of HOA, both the recording and the reproduction are done using a spatial discrete grid in place of spatially continuous formulation. This section intends to illustrate the impact of spatial sampling on HOA performances. Different forms of sampling can be chosen, directly influencing the result. In this report only the Lebedev sampling will be developed.

The discretisation step introduces spatial aliasing at capture [10] and restitution [11]. This aliasing is frequency dependent. For the capture step, this lead to an aliasing frequency for the microphone which compromise the estimation of Ambisonic components at high frequencies.

3.3.1 Encoding

For practical applications, the recording of a sound field within an Ambisonics paradigm cannot be achieved using an infinite continuous distribution of microphones, but using a finite number. Thus the B_{mn} coefficients will also be limited. They will then only describe a part of the spatial extent of the sound field.

The main drawback of the discretisation is the introduction of spatial aliasing and truncation in the Fourier-Bessel expansion which may breaks the quadrature rule. Using a weighted quadrature rule approach, the discretisation consists of an estimation of the continuous integrals over the sphere with weighted sums over a finite number of samples. These integrals should be computed as accurately as possible with only a finite number of samples over a spherical surface.

Let Φ be a function in L^2 . On the unit sphere, a quadrature rule J is defined as the discrete approximation:

$$J(\Phi) = \sum_{l=1}^N w_l \Phi(\theta_l, \sigma_l) \approx \frac{1}{4\pi} \int_{\theta=0}^{2\pi} \int_{\sigma=-\frac{\pi}{2}}^{\frac{\pi}{2}} \Phi(\theta, \sigma) \cos(\sigma) d\theta d\sigma. \quad (3.11)$$

When $\Phi = \tilde{Y}_{mn}(\theta_l, \sigma_l) \tilde{Y}_{m'n'}(\theta_l, \sigma_l)$, the result should be:

$$\sum_{l=1}^N w_l \tilde{Y}_{mn}(\theta_l, \sigma_l) \tilde{Y}_{m'n'}(\theta_l, \sigma_l) = \delta_{mm'} \delta_{nn'} + \eta(n, m, n', m'), \quad (3.12)$$

N represents the number of nodes on the spherical surface, w_l are the weights “introduced to support the equality” [10].

Considering a perfect sphere, the error $\eta(n, m, n', m')$ should be null, but for a real mesh grid it will induce aliasing.

The aliasing can be quantified using the orthogonality error η of eq 3.14 can be displayed in matrix form:

$$D = I - Y^T W Y \quad (3.13)$$

Where I is the $L \times L$ identity matrix, Y is the matrix of spherical harmonics $N \times L$ evaluated at the different nodes of the grid and W is the matrix of weights $N \times N$ from Lebedev rule. Complex transposition is indicated by superscript T .

The Fig. 3.5 shows the orthogonality error D for the Lebedev grid with 50 nodes. The aliasing present in the matrix are errors due do activation of superior orders

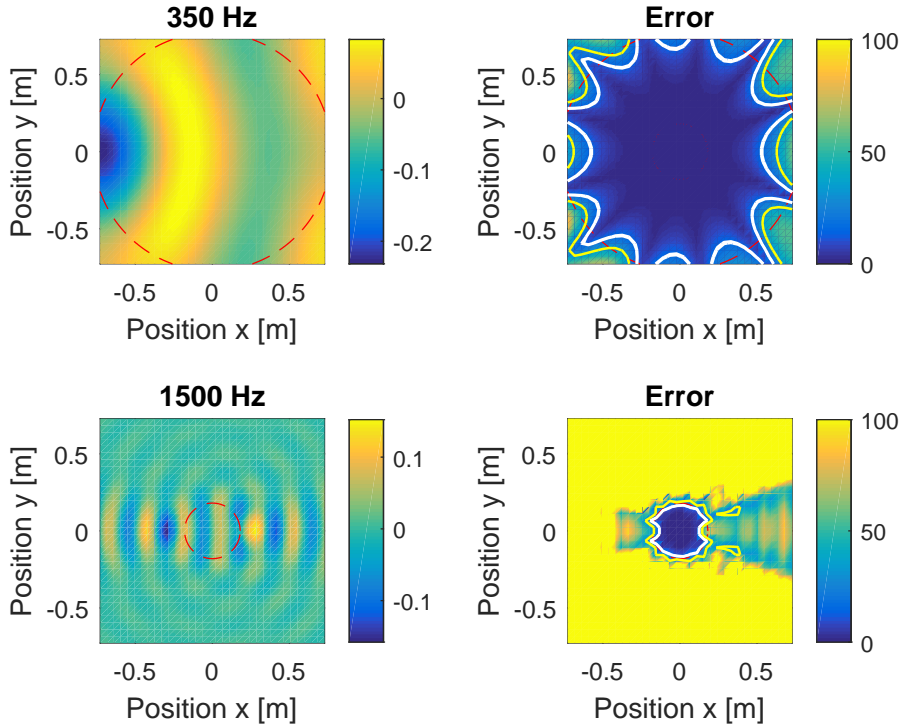


Figure 3.6: Real part of the pressure in Pa from a simulation of a monopole source recorded by spherical microphone at 350 Hz (up) and 1500 Hz (down) with their relative error to a real monopole in percent on the right, program link .

of spherical harmonics into lower orders. This is the order limitation for the order encoding. In this report, the order is limited to 5 in order to avoid colour points that represent aliasing for higher orders. If the selected highest order is larger than 5, aliasing will appear.

The Fig. 3.6 shows results of processing simulations for the case of a recorded sound field created by a monopole source located in $r = 1.07, \theta = 90, \sigma = 0$ using the proposed spherical microphone array geometry, which provides exact integration of spherical harmonics products up to order $m=5$ in (3.12).

The red contour shows the region defined by $kr = M$, k being the wave number, $M = 5$ the order of truncation and r the expected accurate reproduction area defined by Ward and Abhayapala [12]. The white contour shows the normalised error at 15 % defined by:

$$erreur_N(z) = \frac{|p(z) - \hat{p}(z)|^2}{|p(z)|^2} 100, \quad (3.14)$$

where $p(z)$ is the target field and $\hat{p}(z)$ the measured field. It is found that the more the frequency increase, the more the accurate reconstruction area is reduced. This is a common behaviour of Ambisonics explained with more details in Sec. 3.4.

As the information outside of the red circle is not a region of interest, the measurement will be shown only inside in Sec. 5.3

3.3.2 Signals decoding: Basic decoding methods

The basic decoding method focuses on recreating with an array of loudspeakers a sound field over a given area. It contains the spatial information derived from the spherical harmonics representation B_{mn} . For the direct problem, the goal is to recreates B_{mn} with L speakers driven by $s_1 \dots s_L$. This can be formulated in matrix form as follows:

$$Cs = b, \quad (3.15)$$

$$\text{with } C = \begin{bmatrix} Y_{00}(\theta_1, \sigma_1) & Y_{00}(\theta_2, \sigma_2) & \dots & Y_{00}(\theta_L, \sigma_L) \\ \vdots & \vdots & \vdots & \vdots \\ Y_{11}(\theta_1, \sigma_1) & Y_{11}(\theta_2, \sigma_2) & \dots & Y_{11}(\theta_L, \sigma_L) \\ \vdots & \vdots & \vdots & \vdots \\ Y_{mn}(\theta_1, \sigma_1) & Y_{mn}(\theta_2, \sigma_2) & \dots & Y_{mn}(\theta_L, \sigma_L) \end{bmatrix}, s = \begin{bmatrix} S_1 \\ S_2 \\ \vdots \\ S_L \end{bmatrix}, b = \begin{bmatrix} B_{00} \\ B_{11} \\ \vdots \\ B_{mn} \end{bmatrix},$$

where L is the number of loudspeakers, the matrix C contains the spherical harmonics vectors associated to the different speakers position, s is the vector containing the signals of the different loudspeakers and b is the matrix containing the HOA signals.

An exact solution can be found if the number of loudspeakers is superior or equal to the number of HOA signals ($L \geq K_{mn} = (M + 1)^2$). The exactness of the solution depends on the property of C . Thus if now one knows the B_{mn} signals and looks for the driving signals, the inverse problem to solve is formulated as follows:

$$s = D.b, \quad (3.16)$$

with

$$D = C^T \cdot (C \cdot C^T)^{-1} \quad (3.17)$$

D will be called the decoding matrix, due to the fact that HOA signals are obtained from it.

3.4 Ambisonics reconstruction of a spherical source

Using a simulated encoding and decoding, this section aims to show the different limitations of the Ambisonics reproduction.

In a similar way to Sec. 3.3.1 with the microphones discretisation , the arrangement of 50 loudspeakers is a discretisation of the continuous formulation.

Here the aliasing will restrict the decoding order to 5 of the Fourier-Bessel truncation, if not the field reconstructed will be distorted by the aliasing.

The acoustic field from a spherical wave generated by a point source located at a finite distance r_s from the origin is written as:

$$p_s(r) = S \frac{e^{-ik(r-r_s)}}{|r - r_s|}, \quad (3.18)$$

where S is the amplitude of the signal and r is the observation point.

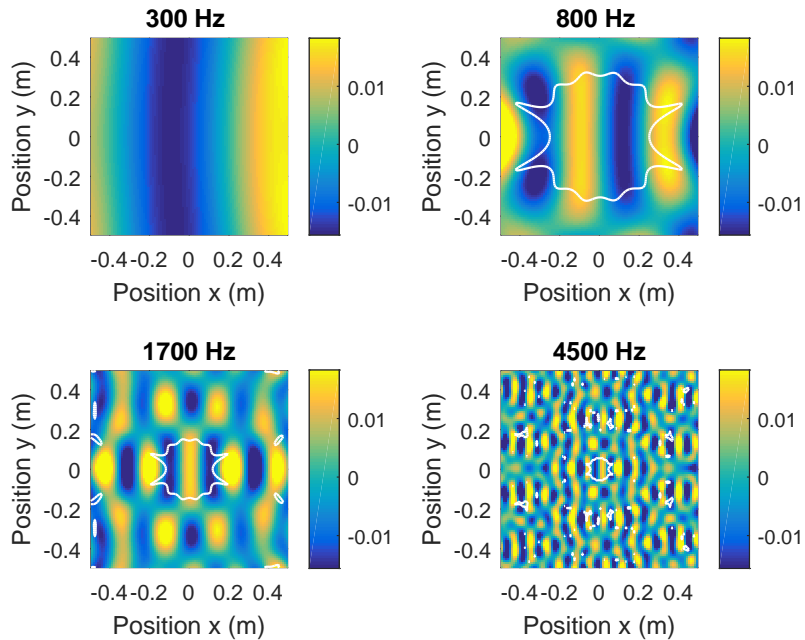


Figure 3.7: Real part of reconstructed spherical wave for a set-up made of 50 loudspeakers arranged on a Lebedev grid with $M = 5$ showing the effect of frequency on the sound field, for a plane in $z = 0$, in Pa, source located at $r = 1.07$, $\theta = -90$ deg, $\sigma = 0$, program link.

Using Fourier-Bessel series as introduced in Sec. 2.2, it is possible to find the Ambisonics signals for a spherical wave (full demonstration in Appendix A.2):

$$B_{mn} = F_m(kr_s)\tilde{Y}_{mn}(\theta_s, \sigma_s) \quad (3.19)$$

with

$$F_m(kr_s) = -i^{(-m+1)} \frac{k}{4\pi} H_m^{(2)}(kr_s), \quad (3.20)$$

where the functions $H_m^{(2)}$ are the spherical Hankel divergent functions of order m . The loudspeakers signals are then calculated using the basic decoding method explained before.

Figures 3.7 and 3.8 show simulations that highlights the general behaviour of the Ambisonics set-up.

Accurate reconstruction, shown as the area circumscribed by the contour line, is centered at the origin. The reconstruction accuracy is impacted by two factors: the frequency and truncation order of Fourier-Bessel series. The influence of the former factor is shown in Fig. 3.7 where one observes that the reconstruction area decrease with frequency.

For the latter factor, Fig. 3.8 shows that when the order M is rising to the limit imposed by the meshing of the reproduction set-up, the reconstruction area is increased.

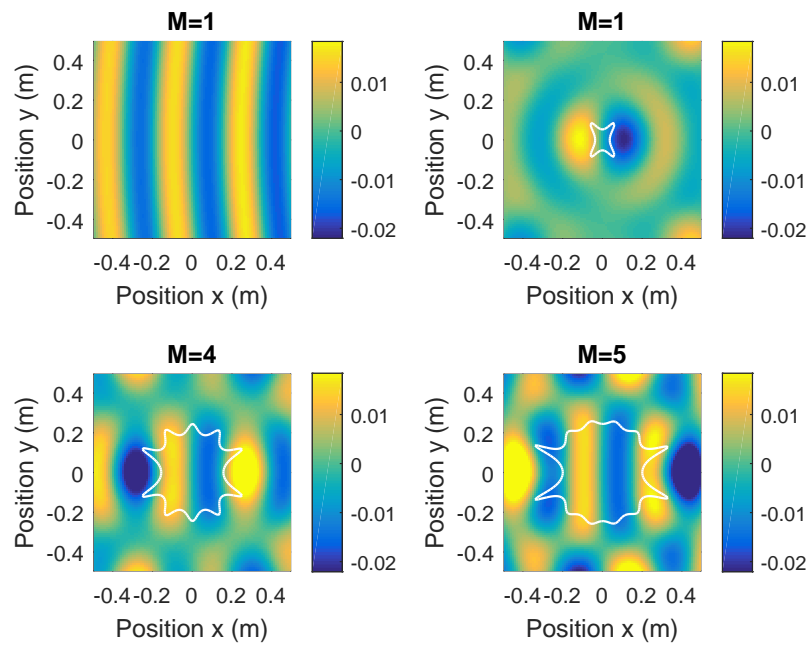


Figure 3.8: Real part of reconstructed spherical wave for a set-up made of 50 loudspeakers arranged on a Lebedev grid with $f = 1000$ Hz showing the effect of truncation order on the sound field, for a plane in $z = 0$, in Pa, source located at $r = 1.07$, $\theta = -90$ deg, $\sigma = 0$, program link.

Chapter 4

Experiments: Materials and methods

This chapter is aimed at the presentation of the material and methods used for the experiments.

As the purpose of the measurements is the comparison of the measured reproduced sound field derived from a reference target sound field, a special attention will be given to explain how the signals are conditioned.

4.1 Uniform rectangular microphone array

Fifty five microphones WN61A were used and connected to three custom microphone preamplifiers, microphone signals are then digitalized using ADA8200 by Behringer and then finally digitally recorded using ADAT to MADI converter ADI648. The recording and playback is done in the DAW (Digital Audio Workstation) Ardour. The specification of the antenna can be found in Appendix B.2, the figure 4.1 shows the antenna.

The uniform rectangular microphone array will be used to measure sound pressure field in order to assess the good reproduction of the Ambisonics system.

4.2 Spherical microphone array

The Memsbedev is a prototype of a spherical recording array developed in the context of Pierre Lecomte's PhD by CINELA¹/ LE CNAM². It's based on the repartition of 50 mems microphones SPH0611LR5H-1 around a sphere with a radius $r = 0.07$ cm according to the Lebedev quadrature.

The spherical microphone array allows the calculation of the sound pressure field, thanks to the combination of the microphone signals on its surface. The description is valid in a spherical region around the microphone which size is frequency dependent.

The Memsbedev is powered by an IEPE³ supply. It is digitalized using the same hardware than for the uniform rectangular microphone array described in Sec. 4.1. As the spherical microphone array position is important to ensure that the decoded sound pressure field from initial recordings is in the same axis than the target sound field, laser pointers were used to accurately place the spherical microphone array in

¹<http://www.cinela.fr>

²Conservatoire national des arts et métiers

³Integrated Electronic Piezoelectric

the center of the loudspeaker array.

The primary use for the spherical microphone array is the computation of equalization filters for active room compensation. It is also used for the measurement and assessment of target and reproduced sound fields. However, as this spherical microphone array is not widely used and still partly unknown, the target and reconstructed sound pressure fields were measured using the uniform rectangular microphone array for comparison and validation. Both results will be compared and discussed.

4.3 Microphone calibration

Due to the microphone amplifier, pre-amplifier and capsule sensitivity, the sensitivity of each channel is different (both plane microphone array and spherical microphone array). Thus a calibration with a calibrator emitting a 1 kHz sine wave at 1 Pa was performed. The RMS (Root-Mean-Square) value of the temporal recorded signal was used for the identification of microphone sensitivity (Pa per digital units). As it is often the case for acoustical measurements in industrial or research context, it is assumed that the microphone pre-amplifier chain presents a flat frequency response.

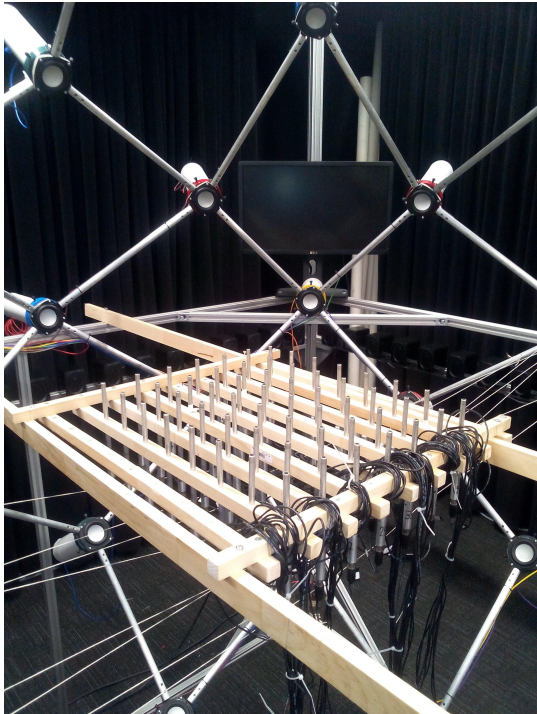


Figure 4.1: Antenna set-up.



Figure 4.2: Calibration of the Membedev microphone.

4.4 Post-processing of recorded signals

As the aim of the measurement is to compare different sound field in the frequency domain, an exponential sweep signal from 0.01 Hz to 24 kHz ($\frac{F_s}{2}$) of ten cycles is generated as input signal.

The measurement signals obtained either from the spherical microphone array or the uniform rectangular array are scaled using the calibration sensitivity described above and used as outputs of the measurement system. The frequency response function (FRF) is obtained from ratio of the output signal in the frequency domain over the input signal in the frequency domain with averaging for the 10 cycles.

The resulting impulse responses are obtained by inverse Fourier Transforms of the FRF cleaned by a half Tukey window.

For temporal analysis, signals are low pass filtered to remove frequency content that might suffer from spatial aliasing occurring for the different configurations. The cut off frequency is 2000 Hz for a direct incidence and 1300 Hz for a sided incidence.

4.5 Results for the spherical microphone array measurements

From the B_{mn} coefficients calculated as shown in section 3.1.1, it is possible, with Eq. 2.3, to evaluate the sound pressure field in extended area for its assessment. It is, however, restricted to the origin-centered area limited by the truncation order M .

As, in this case, the spherical grids used for the recording and reproduction of sound field are identical, the red circles shown in the forthcoming figures indicates in which area the recording and reproduction should theoretically be accurate. The size of the plot will be adapted to this circle as the information outside is less relevant.

Overcoming the spherical array limitations

As mentioned in Sec. 3.1.1, the actual implementation of spherical microphone arrays recording introduces several issues. Indeed, it requires (due to the rigid sphere equalisation filters from Eq. (A.4)), an unacceptable gain at low ka for order > 0 . The higher the order of truncation M is, the stronger the amplification will be, as shown in the dashed lines in Fig. 4.3. This is due to the fact that at low frequency, the first orders are predominant in the sound field, and the estimation of higher orders requires extra amplification of the signals.

This estimation problem is typically ill-conditioned and require regularisation for practical implementation. Accordingly, a proposed method limits the increase of the filters up to a fixed maximum gain, as explained in Moreau [13], in order to regularise the equalisation filters Fh_m , the Tikhonov filters are implemented:

$$E_m(kR) = \frac{Fh_m(kR)^*}{|Fh_m(kR)|^2 + \lambda^2}, \quad (4.1)$$

where $Fh_m(kR)^*$ is the complex conjugate of $Fh_m(kR)$.

The choice of the regularisation parameter λ is linked to maximal linear amplification gain a defined by:

$$\lambda = \frac{1 - \sqrt{1 - 1/a^2}}{1 + \sqrt{1 - 1/a^2}}, \quad (4.2)$$

with $a > 1$.

The factor a can be set equal at all orders M , only taking into account the background noise amplification of the microphones:

$$a = 10^{\frac{a_c}{20}}, \quad (4.3)$$

a_c being the maximal amplification allowed in dB in the resulting HOA signals.

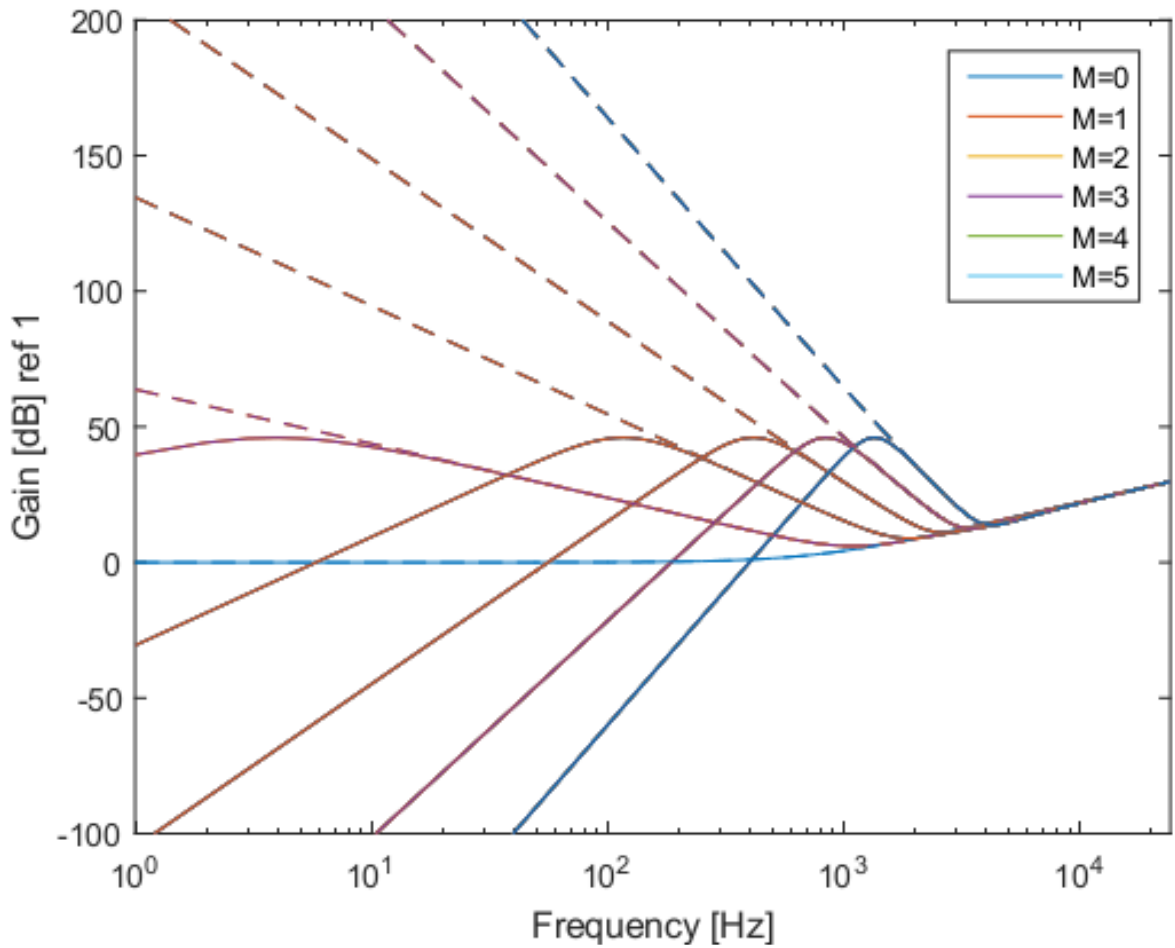


Figure 4.3: Rigid-sphere equalization filters. Theoretical filters as dashed lines. Regularized equalization filters (using Tikhonov regularization) as solid lines, $\lambda = 0.0025$, program link.

Chapter 5

Experiments in an anechoic environment

This chapter aims to shows the different results obtained for the measurements of the Ambisonics set-up in the anechoic chamber.

Results will be shown for the uniform rectangular microphone array and for the spherical microphone array.

In order to observe the behaviour of the Ambisonics set-up, two configurations of sources that create the target sound fields were used for the reported experiments:

1. a source situated in the Ambisonics set-up. This case allows the neglection of the near-field filter and allows to be accurate in the position of the source to generate an Ambisonics source.
2. a source located outside the Ambisonics grid.

For these two configurations, three different measurements are performed:

- A logarithmic swept sine is sent to a real loudspeaker placed in the two locations mentioned above. They are considered as monopole source. This recorded target sound field is used for the two other measurement described below.
- From the first measurement with the spherical microphone array, the signals are encoded and decoded on the Ambisonics set-up. The resulting reproduced sound field is measured using both array. This second measurement allows the observation of the reproduced sound field.
- The original source location is simulated with the Ambisonics theory and decoded with the set-up. This result allows for the evaluation of panning using Ambisonics.

The comparison of these measurements will complete the overall physical assessment of the Ambisonics system performance.

The Matlab program used for these measurement are given in the following link :
[Github link](#)

5.1 Uniform rectangular array measurements: Time-domain approach

A first look is taken in temporal domain one is done by viewing the microphone of the center #29. Figure 5.1 shows the comparison between target source, decoded source and simulated source.

It can be observed for both target and source the peaks arrive at the same time, confirming a good time reproduction and look similar. This confirm an accurate

delay reproduction. However, for the decoded sound, there is a delay induced by the hardware. One needs an estimation of this latency in order to perform time alignment of the signals. This is discussed in the forthcoming.

Figure 5.2 shows the time arrivals of each peaks from the impulse responses for each microphone. It can be observed that the separation (delay in this case) for each row of microphones fits the microphone row separation (2.5 inches, corresponding to 9 samples). It can be seen the delay of each configurations stay constant for all microphones, generalising the fact that there is a constant delay the configurations. This plot also helps in the determination of the source location from the curve of each row of microphones (left direction of Fig.5.2 in this case).

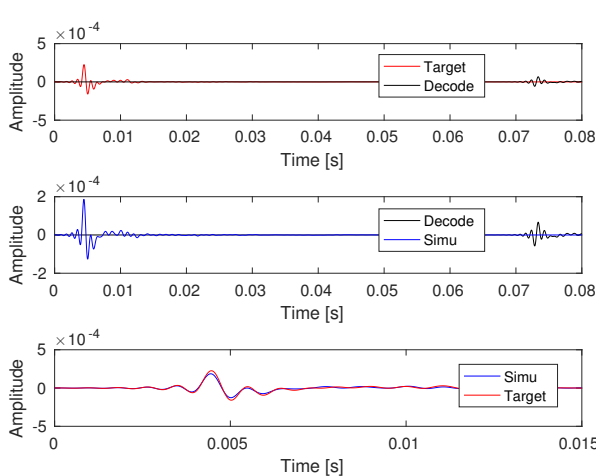


Figure 5.1: Temporal view of microphone 29.

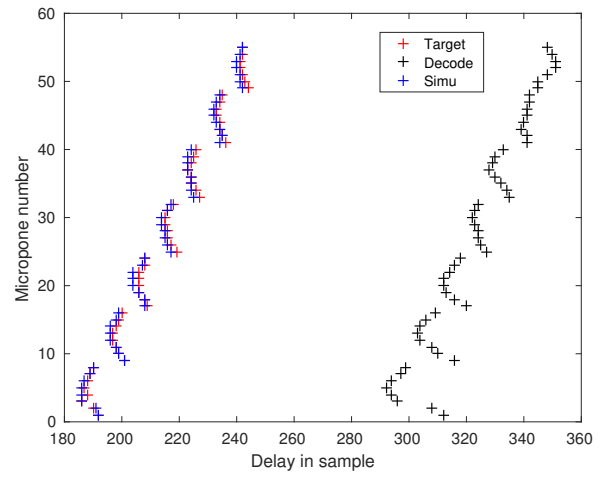


Figure 5.2: Peak location of each microphone (Decode value shifted to see the shape).

5.2 Uniform rectangular array: Frequency-domain approach

The purpose of this section is to compare field at different frequencies and observe if the Ambisonics set-up acts as expected.

The different Figs will present the three measurements: the target on the left recorded from a real source, the decoded source on the uniform rectangular array from the encoding of the target with the spherical array in the middle and the simulated encoding of the source decoded on the set-up.

For the purpose of having a microphone at the origin, the uniform rectangular array has been translated so that microphone #29 is located at the coordinate system origin. It is reminded that the origin corresponds to the ideal listening spot.

The time latency between the measurements is compensated by a mean delay shift. The overall gain is compensated for the decoded sound field (middle column in the figures) by a single factor for the entire grid of points using a Least Mean Square (LMS) method between the target field and the other field.

The white contour show the relative error defined before at 15 percent while the yellow one shows at 30 percent like presented in Equation (3.14) .

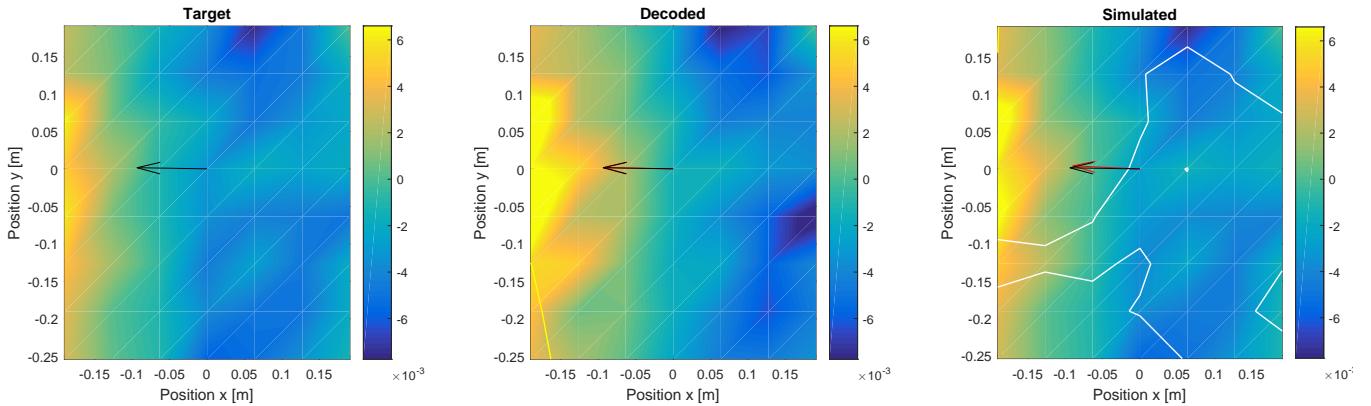


Figure 5.3: Real parts of the recorded sound pressure field at the uniform rectangular array at 500 Hz. Original source at $r = 1.07$, $\theta = 90$, $\sigma = 0$.

The arrows in the middle of the field shows the mean direction of the energy calculated from :

$$I = \frac{1}{2} \Re(pv^*), \quad (5.1)$$

where p is the pressure and v^* the complex conjugate of the velocity. The target arrow is presented in black, the measured decoded field and simulated decoded field in red. The superimposition of both arrows allows a fast visual indicator to see if the wave front is well reconstructed.

It has to be noted that the center should always has the same phase but it can clearly be seen that it is moving. Furthermore the phase move at different speed leading in mistakes in relative error, it is however unknown why.

Figures 5.3 to 5.6 show the results of measurements for a source located on the Lebedev grid ($r = 1.07\text{m}$, $\theta = 90$ deg, $\sigma = 0$ deg).

It can be observed that from 500 Hz to 2000 Hz the wave front is well reconstructed several areas of accurate reproduction are corresponding to less than 30 % of relative error. However, as expected, as the frequency increases the error also increase and the performance of the system is reduced.

Albeit being excellent in the shape of the wave front, error of reproduction was also expected in the anechoic room since few reflective surfaces remain. Also, loudspeakers and microphones do not have perfect gain and phase response. Finally, because of the loudspeaker driving piston size, it was also expected that the loudspeakers do no longer act as perfect monopole for the higher frequency range.

The selected frequency were first limited by the antenna set-up. First, below 200 Hz, due to the size of the uniform rectangular microphone array, the wave front would not have been visible. Above 2300 Hz, spatial aliasing at the microphone array appears and the set-up performance are then not possible to assess.

Next, Figures 5.7 to 5.9 show the measurement results for an orginal source located outside the Lebedev grid of reproduction sources at ($r = 2.23\text{m}$, $\theta = 73$ deg, $\sigma = 12.8$ deg).

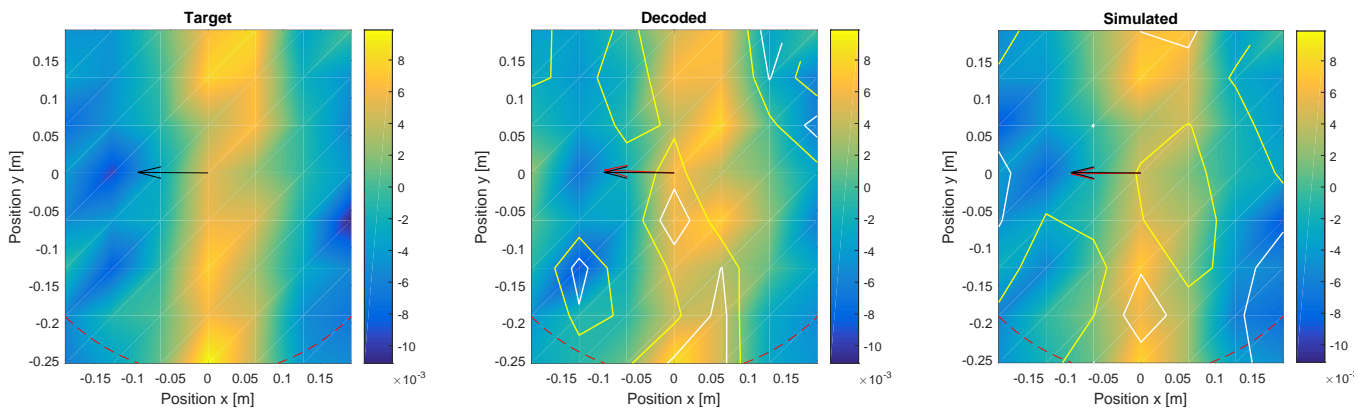


Figure 5.4: Real parts of the recorded sound pressure field at the uniform rectangular array at 1000 Hz. Original source at $r = 1.07, \theta = 90, \sigma = 0$.

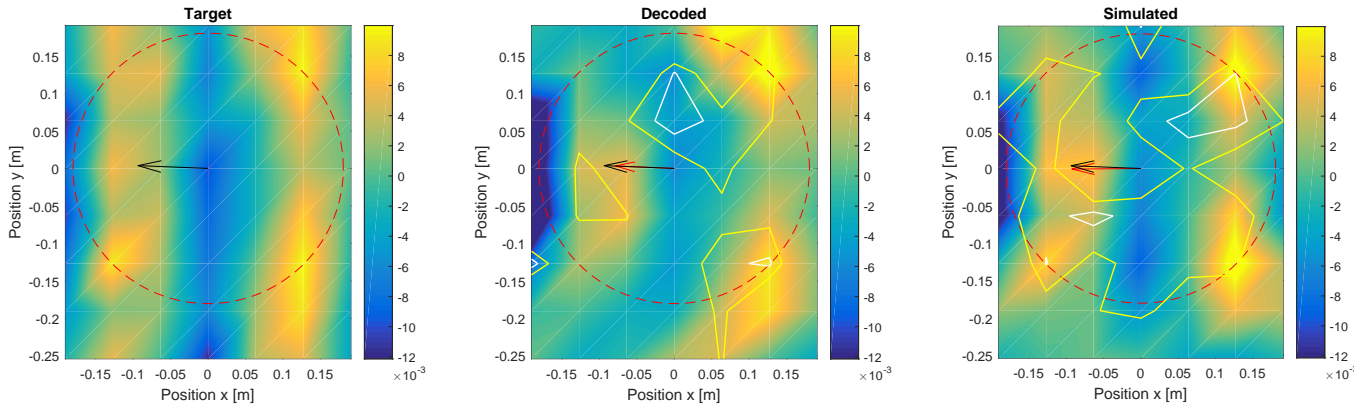


Figure 5.5: Real parts of the recorded sound pressure field at the uniform rectangular array at 1500 Hz. Original source at $r = 1.07, \theta = 90, \sigma = 0$.

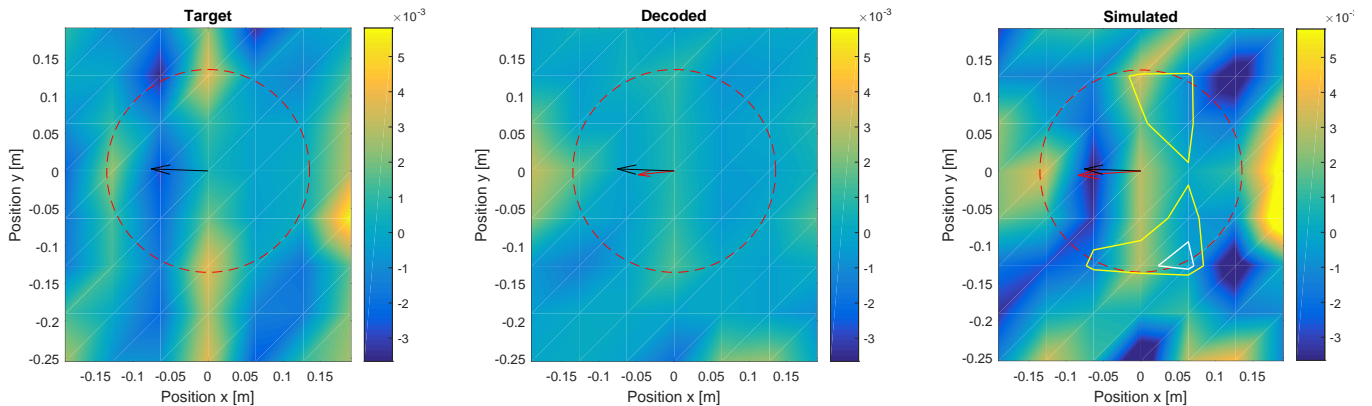


Figure 5.6: Real parts of the recorded sound pressure field at the uniform rectangular array at 2000 Hz. Original source at $r = 1.07, \theta = 90, \sigma = 0$.

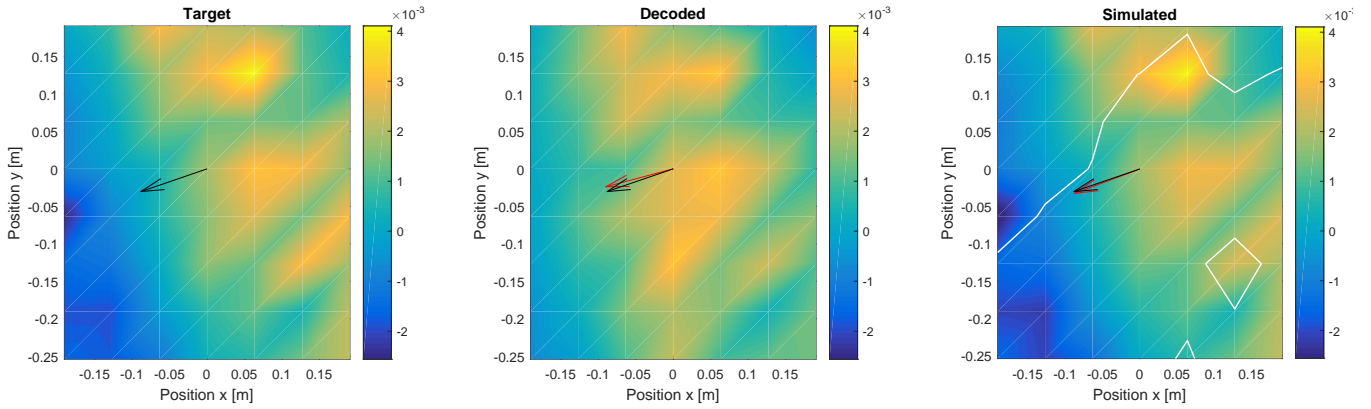


Figure 5.7: Real parts of the recorded sound pressure field at the uniform rectangular array at 500 Hz. Original source at $r = 2.23m$, $\theta = 73$ deg, $\sigma = 12.8$ deg.

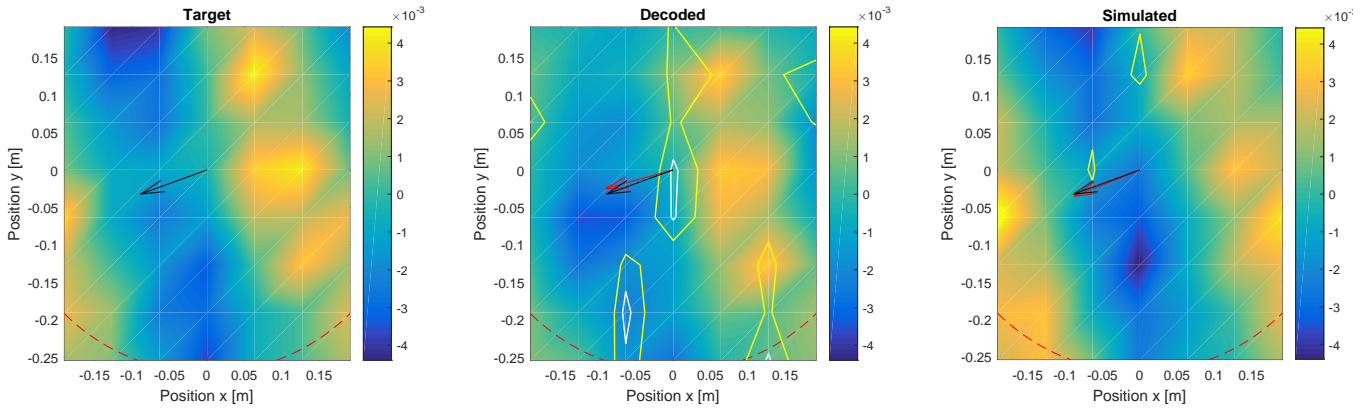


Figure 5.8: Real parts of the recorded sound pressure field at the uniform rectangular array at 1000 Hz. Original source at $r = 2.23m$, $\theta = 73$ deg, $\sigma = 12.8$ deg.

Similar comments apply. However, due to the angle of the original source with respect to the uniform rectangular microphone array, the spatial aliasing appear for a lower frequency. Thus, the field at 2000 Hz cannot be used for accurate assessing. It is therefore not included in this report. Only the Fig. 5.9 seems to be bit different the decoded field seems to be lower than the target, this is probably related to the LMS method applied to the field which take into account the whole uniform rectangular array, thus the presence of the inaccurate part which may contains high level.

Based on the reported measurements using the uniform rectangular array of microphones, it is concluded that the Ambisonics set-up is able to perform accurate sound field reproduction in the spatial and frequency domain of interest. In comparison with the measurements performed with the spherical microphone array, as reported in the next section, the measurements using the rectangular uniform microphone array does not include any post-processing, therefore it is considered as a stable validation basis for further comparison with the measurements of reproduced sound field using the spherical microphone array.

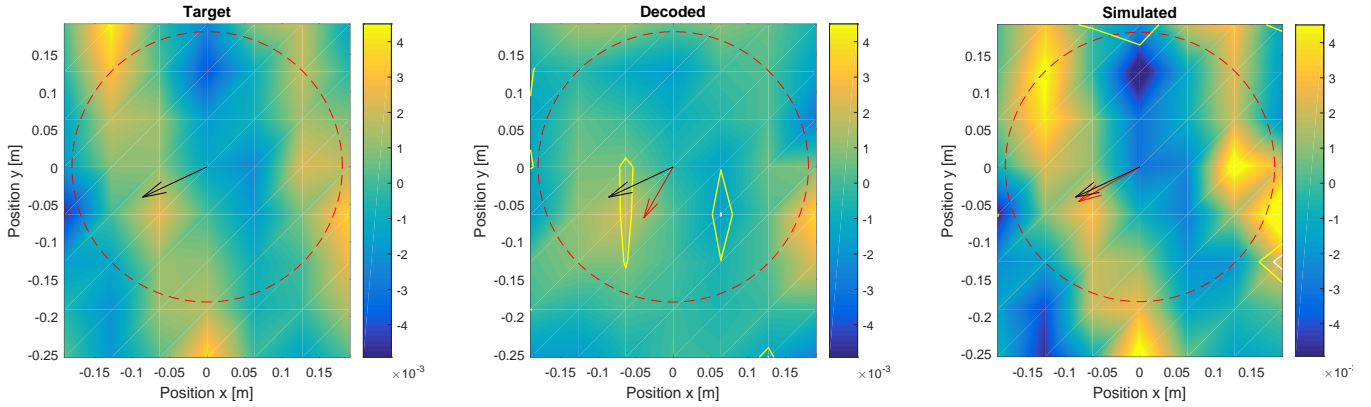


Figure 5.9: Real parts of the recorded sound pressure field at the uniform rectangular array at 1500 Hz. Original source at $r = 2.23\text{m}$, $\theta = 73$ deg, $\sigma = 12.8$ deg.

5.3 Spherical microphone array

As it was done in the previous section using the uniform rectangular microphone array, this section will show sound fields inside the Ambisonics set-up. However, this time the results are based on measurement using the spherical microphone array. Figures 5.10 to 5.12 show the first configuration (described in beginning of Chap. 5) and the Figures 5.13 to 5.16 show the second (described in beginning of Chap. 5).

It is reminded that the filters using Tikhonov regularization are used to reduce the noise amplificationn. Therefore, the red circle is not an accurate predictor of reconstruction area. Because of these regularization filters, the reconstruction area should be smaller for the lower frequencies. The error contour is the same as before, the white contour show the relative error defined before at 15 percent while the yellow one shows at 30 percent like presented in Equation (3.14), thus in order see where is the minimum of the error one has to look which colour is inside the other. For example in Fig. 5.10 simulated field, the white is inside while the yellow outside, thus the center is the best area reconstructed.

The measurements based on the spherical microphone array proves to be similar to the results obtained for the uniform rectangular microphone array. Hence validating both measurement methods and set-up. However, as explained earlier a phase shift can be observed, particularly in the Fig 5.10 with the decoded field, increasing the relative error.

The decoded field from the measurement appear to be more twisted than the simulated one. This is probably due to the double recording, the theory assume that the microphones and the loudspeakers are perfectly positioned which is not, these errors are present twice in this measurement.

Therefore, based on the reported reproduced sound fields using the spherical microphone array measurements, the Ambisonics set-up is able to perform accurate sound field reproduction in the expected spatial and frequency regions.

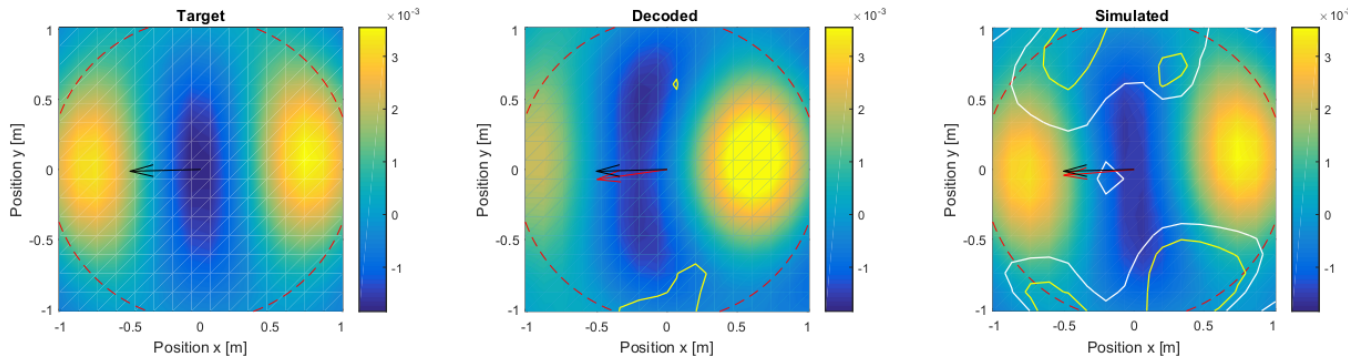


Figure 5.10: Real parts of the extrapolated sound pressure field from spherical microphone array at 250 Hz. Original source at $r = 1.07m, \theta = 90\text{ deg}, \sigma = 0\text{ deg}$.

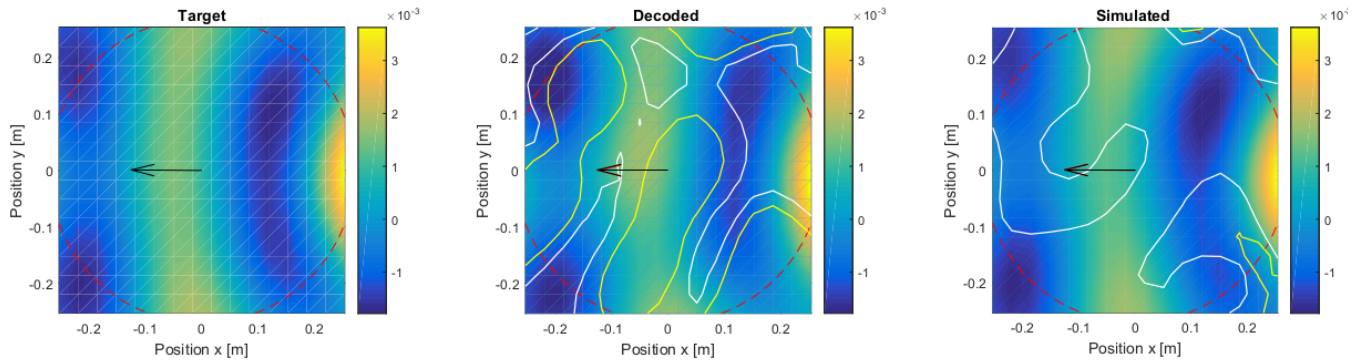


Figure 5.11: Real parts of the extrapolated sound pressure field from spherical microphone array at 1000 Hz. Original source at $r = 1.07m, \theta = 90\text{ deg}, \sigma = 0\text{ deg}$.

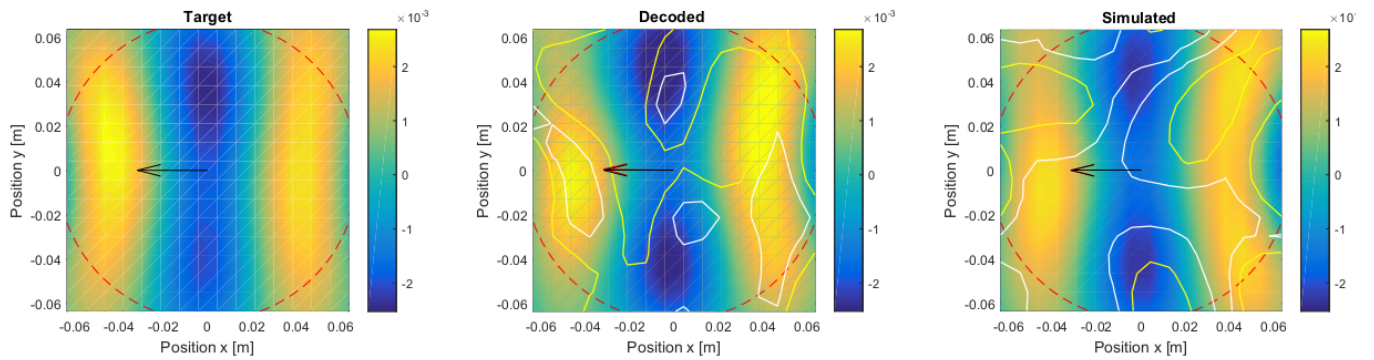


Figure 5.12: Real parts of the extrapolated sound pressure field from spherical microphone array at 4000 Hz. Original source at $r = 1.07m, \theta = 90\text{ deg}, \sigma = 0\text{ deg}$.

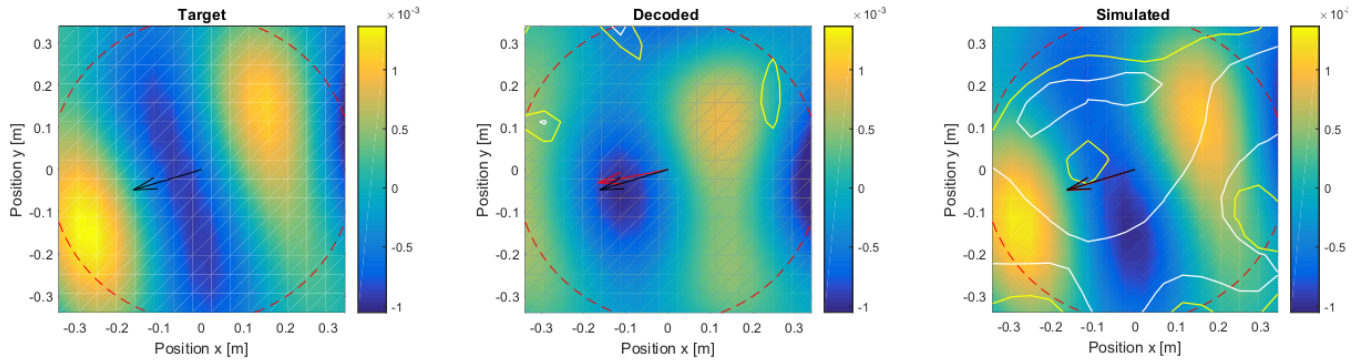


Figure 5.13: Real parts of the extrapolated sound pressure field from spherical microphone array at 750 Hz. Original source at $r = 2.23m, \theta = 73$ deg, $\sigma = 12.8$ deg.

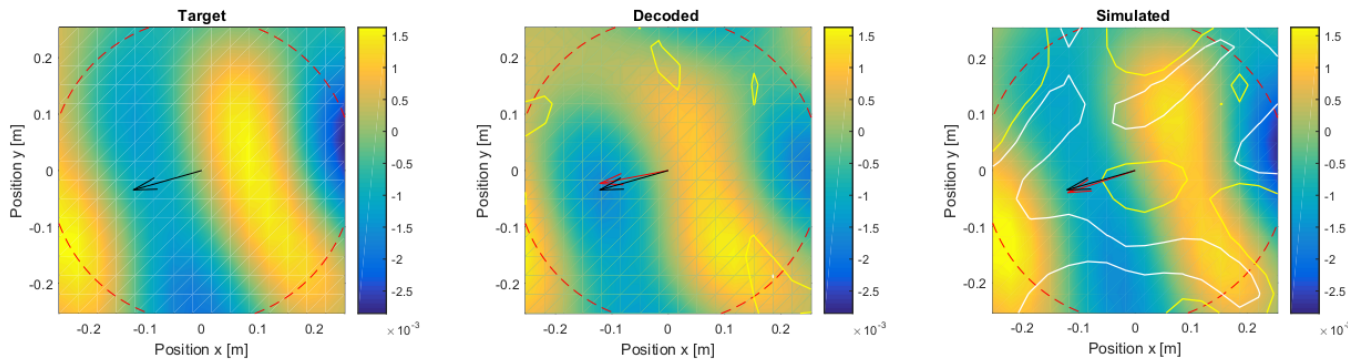


Figure 5.14: Real parts of the extrapolated sound pressure field from spherical microphone array at 1000 Hz. Original source at $r = 2.23m, \theta = 73$ deg, $\sigma = 12.8$ deg.

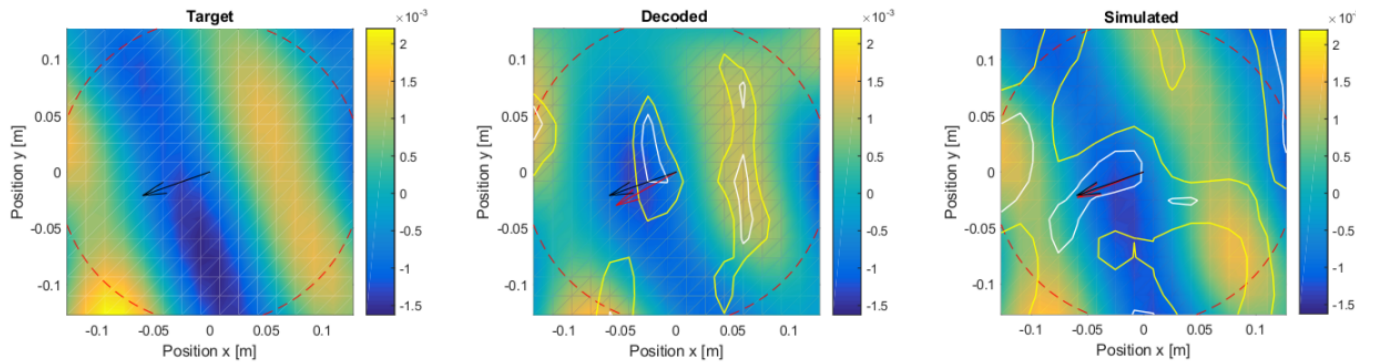


Figure 5.15: Real parts of the extrapolated sound pressure field from spherical microphone array at 2000 Hz. Original source at $r = 2.23m, \theta = 73$ deg, $\sigma = 12.8$ deg.

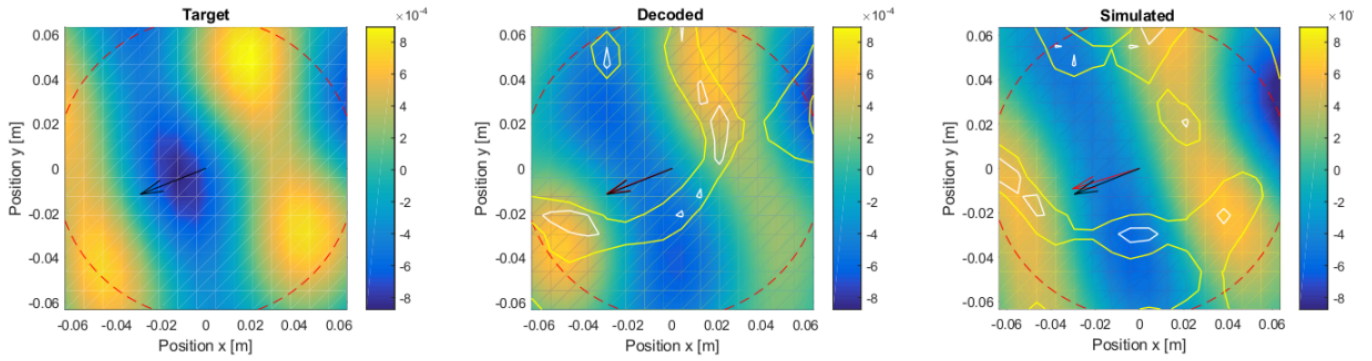


Figure 5.16: Real parts of the extrapolated sound pressure field from spherical microphone array at 4000 Hz. Original source at $r = 2.23\text{m}$, $\theta = 73\text{ deg}$, $\sigma = 12.8\text{ deg}$.

5.3.1 Discussion of Membedev and plane antenna results

As it can now be seen, both measurement systems (uniform rectangular and spherical microphone arrays) provide similar and coherent results. The wave front is well reproduced. However, both measurement systems show different limitations.

On one side, for the uniform rectangular microphone array, the lowest frequency that can be investigated is lower, although it is possible to reduce the spacing in between each microphones to increase the resolution, the size has to be reduced. On the other side, the spherical microphone present a compact solution taking into account its intrusion and diffraction in the impinging sound pressure fields.

The results for the uniform rectangular microphone array show less smooth results due to low spatial resolution with 50 microphones. However, spatial interpolation could solve this limitation. This is a topic of future work.

Chapter 6

Conclusion

The aim of the work and this report was to learn the usage of an Ambisonics method and set-up in order to provide a physical assessment of Ambisonics for sound field reproduction. Ambisonics was assessed both theoretically and experimentally for a set-up made of 50 reproduction sources arranged on a Lebedev grid. The loudspeaker array was an open sphere and the spherical microphone array was a rigid sphere.

The physical assessment of the performance was performed based on two distinct measurement systems: Using a spherical arrangement on microphones and a uniform rectangular microphone array. Based on both measurement systems, it was observed that the wave fronts are well reconstructed. However, the error field was slightly different for both measurement methods.

The first limitation come from the theory itself which consider the system as a perfect one (monopole reproduction sources, perfectly rigid spherical microphone array, etc.). However, the loudspeakers are not perfect monopole, they show a non-flat frequency response function and a potential directivity with increasing frequency. Also, diffraction on surrounding objects occurs and misplacement of transducers is inevitable. These typical factors induce experimental errors. Furthermore, there were phase problems in the record and adjusting afterwards still not provide a very good adequacy, thus it was difficult to compare different sound pressure fields.

Differences between both measurement methods were reported and discussed. The uniform rectangular microphone array shows a shorter frequency range due to the spacing between the microphones. This limitation is reduced with the spherical microphone array, at the cost of supplementary processing. Although, it is possible to adjust the spacing arrangement, the spherical microphone provide a compact shape which also takes into account the diffraction induced by its own presence in the field.

However, due to time constraints it was impossible to implement the method. Therefore, measurements and assessment were only performed and reported for the anechoic room.

Further measurements with an active room compensation and equalisation is planned for a near future in order to compensate gain and phase differences, as well as positioning problems.

This internship allowed to produce a Matlab toolbox to facilitate the extraction of the measurement from the antenna or spherical microphone, as well as producing simulations on HOA.

Chapter 7

Acknowledgement

This chapter aims to thank all the benefactor of this internship. In particularity, Alain berry, Manuel Melon, Philippe-Aubert Gautier et Pierre Lecomte for their help and availability all along the internship.

I would like also to thank all the GAUS team which have welcome me during these 5 months.

Bibliography

- [1] Michael Gerzon. Periphony: With-height sound reproduction. *Journal of the Audio Engineering Society*, 21(1):2–10, 1973.
- [2] Jeffrey Stephen Bamford. *An Analysis Of Ambisonic Sound Systems Of First And Second Order*. PhD thesis, University of Waterloo, 1995.
- [3] Jérôme Daniel. *Representation de champs acoustiques, application à la transmission et à la reproduction de scènes sonores complexes dans un contexte multimédia*. PhD thesis, Ph. D. Thesis, University of Paris VI, France, 2000, <http://gyronymo.free.fr>, 2000.
- [4] Sébastien Moreau. Étude et réalisation d'outils avancés d'encodage spatial pour la technique de spatialisation sonore Higher Order Ambisonics: microphone 3D et contrôle de distance. *École doctorale de l'université du Maine, Le Mans, France*, 2006.
- [5] Filippo Maria Fazi. *Sound Field Reproduction*. PhD thesis, University of Southampton, 2010.
- [6] Pierre Lecomte, Philippe-Aubert Gauthier, Christophe Langrenne, and Alexandre Garcia. Convention Paper 9433 On the Use of a Lebedev Grid for Ambisonics. pages 1–12, 2015.
- [7] Michel Bruneau. *Manuel d'acoustique fondamentale*. Hermès, 1998.
- [8] Earl G Williams. *Fourier Acoustics: Sound Radiation and Nearfield Acoustical Holography*. Academic press, 1999.
- [9] Boaz Rafaely. *Fundamentals of Spherical Array Processing*, volume 8. Springer, 2015.
- [10] Boaz Rafaely, Barak Weiss, and Eitan Bachmat. Spatial Aliasing in Spherical Microphone Arrays. *Signal Processing, IEEE Transactions on*, 55(3):1003–1010, 2007.
- [11] Mark A Poletti. Three-dimensional surround sound systems based on spherical harmonics. *Journal of the Audio Engineering Society*, 53(11):1004–1025, 2005.
- [12] Darren B Ward and Thushara D Abhayapala. Reproduction of a plane-wave sound field using an array of loudspeakers. *IEEE Transactions on speech and audio processing*, 9(6):697–707, 2001.
- [13] Stéphanie Bertet, Jérôme Daniel, and Sébastien Moreau. 3D Sound Field Recording With Higher Order Ambisonics-objective Measurements And Validation Of Spherical Sicrophone. In *Audio Engineering Society Convention 120*. Audio Engineering Society, 2006.
- [14] Milton Abramowitz and Irene A Stegun. Handbook of mathematical functions. ninth printing, 1972.

Appendix A

Appendix

A.1 Demonstration of the integration on a rigid sphere

Assuming a sphere of radius a in an acoustic pressure field, the resulting acoustic pressure field is given by the sum of the direct pressure p_{dir} without the sphere and the diffracted one p_{dif} :

$$p_{tot}(kr, \theta, \sigma) = p_{dir}(kr, \theta, \sigma) + p_{dif}(kr, \theta, \sigma), \quad \forall kr, \theta, \sigma. \quad (\text{A.1})$$

Using Fourier-Bessel series Eq.((2.3)) on both sound pressure fields, they can be written as:

$$p_{dir}(r, \theta, \sigma) = \sum_{m=0}^{\infty} i^m J_m(kr) \sum_{n=-m}^m B_{mn} \tilde{Y}_{mn}(\theta, \sigma), \quad \forall kr, \theta, \sigma, \quad (\text{A.2})$$

$$p_{dif}(r, \theta, \sigma) = \sum_{m=0}^{\infty} i^m H_m^{(2)}(kr) \sum_{n=-m}^m D_{mn} \tilde{Y}_{mn}(\theta, \sigma), \quad \forall kr, \theta, \sigma, \quad (\text{A.3})$$

where the functions $H_m^{(2)}$ are the spherical Hankel function of the second kind. They represent diverging spherical wave from the diffracting object. The resulting pressure can be written as:

$$p_{tot}(r, \theta, \sigma) = \sum_{m,n,\sigma} i^m \tilde{Y}_{mn}(\theta, \sigma) (B_{mn} J_m(kr) + D_{mn} H_m^{(2)}(kr)), \quad \forall kr, \theta, \sigma. \quad (\text{A.4})$$

Then, knowing that the particular velocity is null on a rigid sphere surface:

$$u_{tot}(r = a) = \frac{i}{\omega \rho} \frac{\partial p_{tot}}{\partial r} \Big|_{r=a} = 0, \quad (\text{A.5})$$

it can be written from Eq. (A.4) that:

$$0 = \sum_{n,m,\sigma} \frac{i^{m+1}}{\omega \rho} \tilde{Y}_{mn}(\theta, \sigma) (B_{mn} J'_m(ka) + D_{mn} H_m'^{(2)}(ka)), \quad \forall ka, \theta, \sigma, \quad (\text{A.6})$$

$H_m'^{(2)}(kr)$ being the partial derivative with respect to kr of the spherical Hankel function of the second kind. The same goes for the the Bessel functions, $J'_m(kr)$ is the first derivative of $J_m(kr)$ with respect to kr .

As this equation is valid for all kr, θ, σ . One directly obtains the diffracted coefficients:

$$D_{mn} = B_{mn} \frac{J'_m(ka)}{H_m'^{(2)}(ka)}. \quad (\text{A.7})$$

Then, the total pressure can now be rewritten as:

$$p_{tot}(r, \theta, \sigma) = \sum_{m=0}^{\infty} i^m \left(J_m(kr) - \frac{J'_m(ka)}{H'^{(2)}_m(ka)} H^{(2)}_m(kr) \right) \sum_{n=-m}^m B_{mn} \tilde{Y}_{mn}(\theta, \sigma), \quad \forall kr, \theta, \sigma. \quad (\text{A.8})$$

Finally, using the Wronskian [14]:

$$W\{J_m(x), H^{(2)}_m(x)\} = J_m(x)H^{(2)}_m(x) - J_m(x)H'^{(2)}_m(x) = \frac{-i}{x^2}, \quad (\text{A.9})$$

the pressure on surface of the sphere can written as:

$$p_{tot}(ka, \theta, \sigma) = \sum_{m=0}^{\infty} \frac{i^{m-1}}{(ka)^2 H'^{(2)}_m(ka)} \sum_{n=-m}^m B_{mn} \tilde{Y}_{mn}(\theta, \sigma). \quad (\text{A.10})$$

Thus, B_{mn} coefficients for the impinging and diffracted sound fields can be determined by:

$$B_{mn} = i^{-(m-1)}(ka)^2 H'^{(2)}_m(ka) \langle p(ka, \theta, \sigma), \tilde{Y}_{mn}(\theta, \sigma) \rangle_{3D}. \quad (\text{A.11})$$

A.2 Demonstration of monopole encoding

The acoustic field of a spherical wave generated by a point source situated at a finite distance from the origin is written for the observation point r from the source position r_s as:

$$p_s(r) = S \frac{e^{-ik||r-r_s||}}{4\pi||r-r_s||}, \quad (\text{A.12})$$

Using Fourier-Bessel expansion, as used by Rafaely [9], it is possible to write it likes:

$$p_s(r) = S \frac{e^{-ik||r-r_s||}}{4\pi||r-r_s||} = \sum_{m=0}^{\infty} \sum_{n=-m}^m (-i) \frac{k}{4\pi} H^{(2)}_m(kr_s) J_m(kr) \tilde{Y}_{mn}(\theta_s, \sigma_s) \tilde{Y}_{mn}(\theta, \sigma) \text{ for } r < r_s, \quad (\text{A.13})$$

where $||.||$ is the Euclidean norm.

Recalling that the general solution of the wave equation for interior problem is:

$$p(r, \theta, \sigma, t) = \sum_{m=0}^{\infty} i^m J_m(kr) \sum_{n=-m}^m B_{mn} \tilde{Y}_{mn}(\theta, \sigma) e^{j\omega t}.$$

It can easily be find by analogy from both precedents equations that:

$$B_{mn} = -i^{(-m+1)} \frac{k}{4\pi} H^{(2)}_m(kr_s) \tilde{Y}_{mn}(\theta_s, \sigma_s). \quad (\text{A.14})$$

A.3 Matlab program

The Matlab program are accessible to download in Github.

Appendix B

Appendix Constructions

B.1 Spherical array of loudspeakers

During the internship, I had to finish the Ambisonic sphere of loudspeakers. The structure was already completed, but the loudspeaker enclosures had to be built. The loudspeakers are Aura Sound NS3-193-8A. They had to be inserted in a pipe in order to complete closed-cabinet loudspeakers and insert them in the supporting structure.

Using Akabak software for a rapid evaluation of the cabinets, the lengths of the 3-inch-diameter pipe was set to 31 cm. The resulting volume is 5.7 L. Figure B.1 shows the measured frequency response function of the assembled loudspeaker while being measured at 1 m.

A support was designed to fit the loudspeaker with the tube and avoid acoustic leaks. The part was designed under Solidworks using a waterjet cutting machine. Finally, 50 loudspeakers were built (FigB.2) and the finished spherical array is shown on FigB.3.

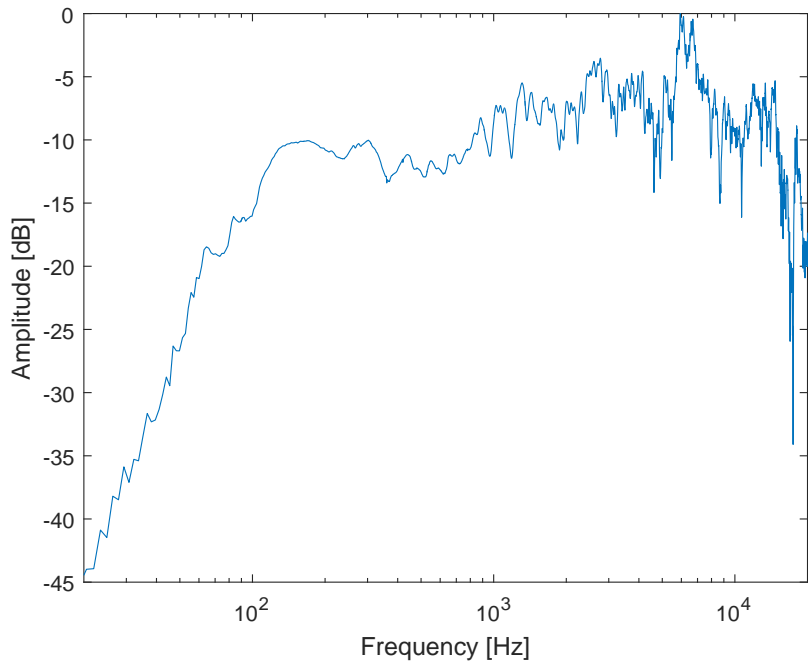


Figure B.1: Normalised measure of the loudspeaker in anechoic room.



Figure B.2: Louspeakers used on the spherical array.



Figure B.3: Ambisonic restitution sphere with 50 loudspeakers.

B.2 Uniform rectangular array

To access the real sound field produced by the Ambisonic set-up without any processing, an uniform rectangular array of microphones was constructed. Figures B.4 and B.5 show the characteristics of the of the rectangular array (inch scaled) and the installed set-up. Due to technical constraints, the final size of the array was 8 by 7 microphones.

The rectangular array is shifted on the side so that microphone #29 is centered at the origin.

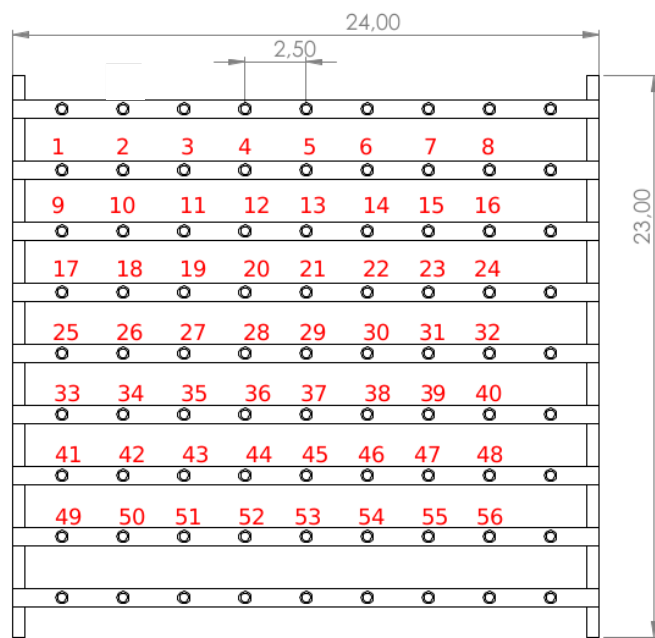


Figure B.4: Scheme of the rectangular array and the position of the microphones. Dimensions are indicated in inches.

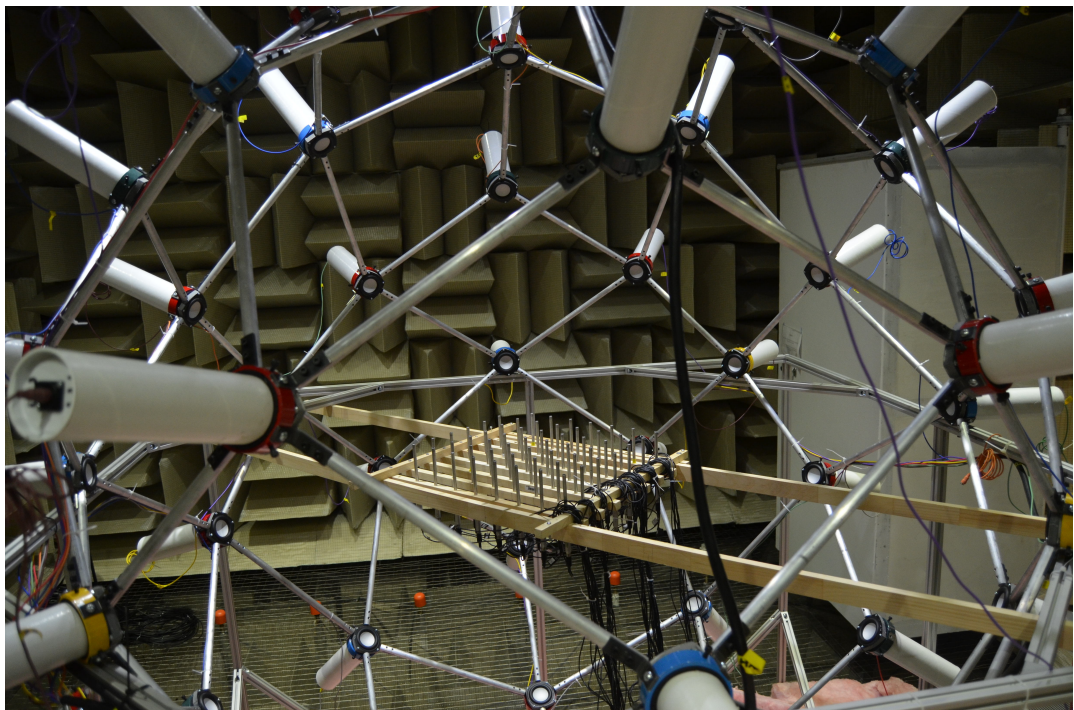


Figure B.5: The uniform rectangular array of microphone disposed in the equatorial plan of the spherical loudspeaker array in the anechoic room.